

See discussions, stats, and author profiles for this publication at: <https://www.researchgate.net/publication/281517334>

# Rational Development of a Potent 15-Lipoxygenase-1 Inhibitor with *in Vitro* and *ex Vivo* Anti-inflammatory Properties

ARTICLE *in* JOURNAL OF MEDICINAL CHEMISTRY · SEPTEMBER 2015

Impact Factor: 5.45 · DOI: 10.1021/acs.jmedchem.5b01121 · Source: PubMed

---

CITATION

1

READS

7

## 6 AUTHORS, INCLUDING:



Frank J Dekker

University of Groningen

64 PUBLICATIONS 1,260 CITATIONS

SEE PROFILE

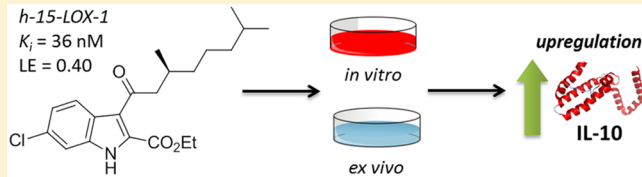
## Rational Development of a Potent 15-Lipoxygenase-1 Inhibitor with *in Vitro* and *ex Vivo* Anti-inflammatory Properties

Nikolaos Eleftheriadis,<sup>†</sup> Constantinos G. Neochoritis,<sup>‡</sup> Niek G. J. Leus,<sup>†</sup> Petra E. van der Wouden,<sup>†</sup> Alexander Dömling,<sup>‡</sup> and Frank J. Dekker\*,<sup>†</sup>

<sup>†</sup>Department of Pharmaceutical Gene Modulation, <sup>‡</sup>Department of Drug Design, Groningen Research Institute of Pharmacy, University of Groningen, Antonius Deusinglaan 1, 9713 AV Groningen, The Netherlands

### Supporting Information

**ABSTRACT:** Human 15-lipoxygenase-1 (h-15-LOX-1) is a mammalian lipoxygenase and plays an important role in several inflammatory lung diseases such as asthma, COPD, and chronic bronchitis. Novel potent inhibitors of h-15-LOX-1 are required to explore the role of this enzyme further and to enable drug discovery efforts. In this study, we applied an approach in which we screened a fragment collection that is focused on a diverse substitution pattern of nitrogen-containing heterocycles such as indoles, quinolones, pyrazoles, and others. We denoted this approach substitution-oriented fragment screening (SOS) because it focuses on the identification of novel substitution patterns rather than on novel scaffolds. This approach enabled the identification of hits with good potency and clear structure–activity relationships (SAR) for h-15-LOX-1 inhibition. Molecular modeling enabled the rationalization of the observed SAR and supported structure-based design for further optimization to obtain inhibitor **14d** that binds with a  $K_i$  of 36 nM to the enzyme. *In vitro* and *ex vivo* biological evaluations of our best inhibitor demonstrate a significant increase of interleukin-10 (IL-10) gene expression, which indicates its anti-inflammatory properties.



### INTRODUCTION

Inflammatory lung diseases like asthma and chronic obstructive pulmonary disease (COPD) can have detrimental effects on patients' health.<sup>1</sup> Fortunately, nowadays, these diseases can be alleviated by various therapeutic agents. Nevertheless, expansion of the therapeutic possibilities is needed because for some patients the currently available medicines are ineffective or cause severe side effects.<sup>2</sup> Therefore, the development of novel compounds targeting enzymes that are involved in inflammatory lung diseases is highly important.

The regulatory function of macrophages is gaining increasing attention in drug discovery because they play key regulatory roles in the different disease stages of asthma and COPD as they polarize into different subclasses according to the cytokines that they encounter in their environment.<sup>3</sup> On the basis of the signals that they receive as well as their role and cytokine profile, macrophages are categorized into three subpopulations: M1 (induced by LPS/IFN $\gamma$ ), M2 (induced by IL-4/IL-13), and M2-like subsets (combination of Toll-like receptor stimulation). M1 macrophages play a role in inflammatory responses to intracellular pathogens, and M2 are involved in scavenging debris, promoting angiogenesis, and helping with tissue remodeling/repair and are therefore considered to be wound-healing macrophages. The third class is M2-like macrophages; as the name implies, these are macrophages that resemble M2. M2-like macrophages are able to produce TGF- $\beta$  and IL-10, implying that they have an anti-inflammatory role.<sup>4–6</sup>

An enzyme class highly expressed in macrophages and other immune cells is the lipoxygenases (LOXs). These enzymes are nonheme iron containing enzymes that metabolize polyunsaturated fatty acids (PUFAs) such as arachidonic acid and linoleic acid into lipid signaling molecules such as leukotrienes and lipoxins.<sup>7–9</sup> Human 15-lipoxygenase-1 (h-15-LOX-1, also denoted 12/15-LOX) is an important mammalian lipoxygenase responsible for the biosynthesis of anti- and pro-inflammatory mediators (signaling molecules) such as lipoxins and eoxins.<sup>10,11</sup> This enzyme is highly expressed in monocytes and broncho-alveolar epithelial cells as well as in eosinophils and macrophages of asthmatic patients.<sup>12–14</sup> Growing evidence suggests that h-15-LOX-1 may modulate inflammatory responses. It was demonstrated that h-15-LOX-1 regulates the expression of IL-12 in a cell-type and stimuli-restricted manner.<sup>15</sup> In addition, in lungs, it has been demonstrated that signaling products of h-15-LOX-1 can stimulate inflammation and mucus secretion.<sup>16</sup> The crucial regulatory role of h-15-LOX-1 in several respiratory diseases such as asthma, COPD, and chronic bronchitis<sup>14,17–20</sup> and in modulating the inflammatory response calls for the development of novel potent and selective inhibitors.

Despite the fact that the key role of h-15-LOX-1 was exemplified in it being a target in drug discovery for several inflammatory diseases, the discovery of very potent h-15-LOX-1 inhibitors and their role as a novel therapeutic strategy is still

Received: July 17, 2015

Published: September 2, 2015

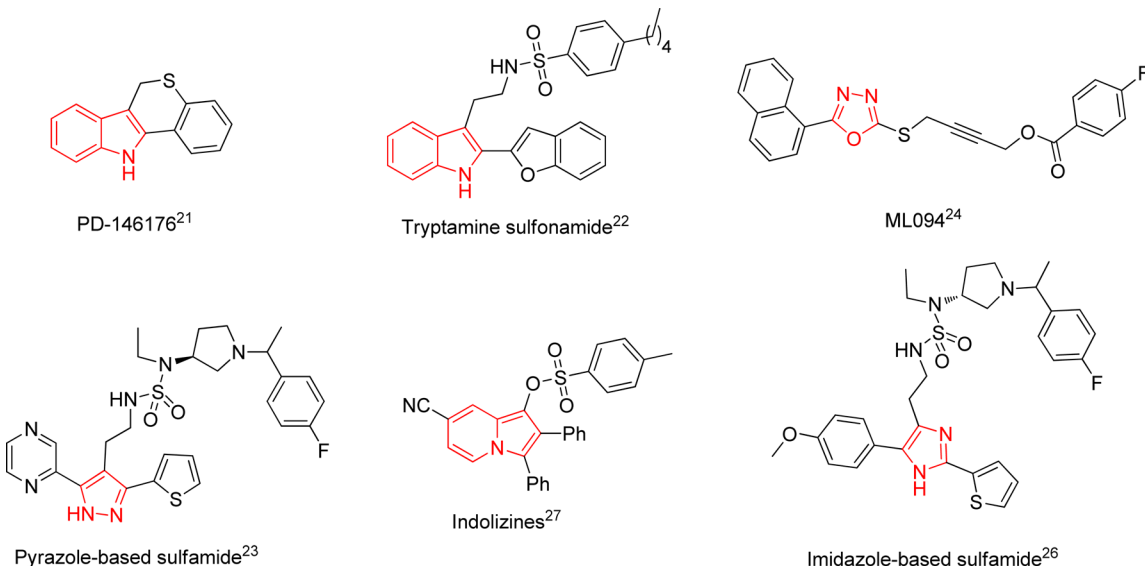


Figure 1. Examples of previously reported 15-LOX inhibitors.

### Substitution Oriented Screening (SOS)

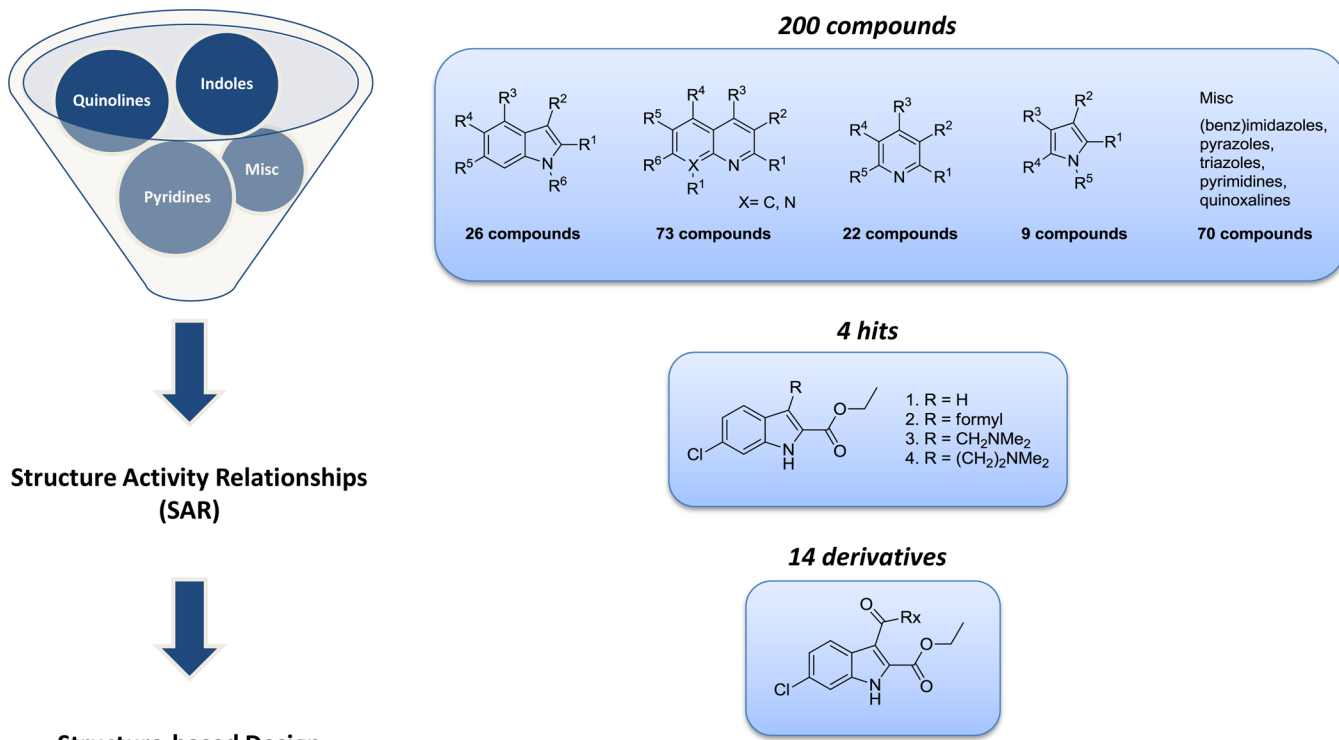
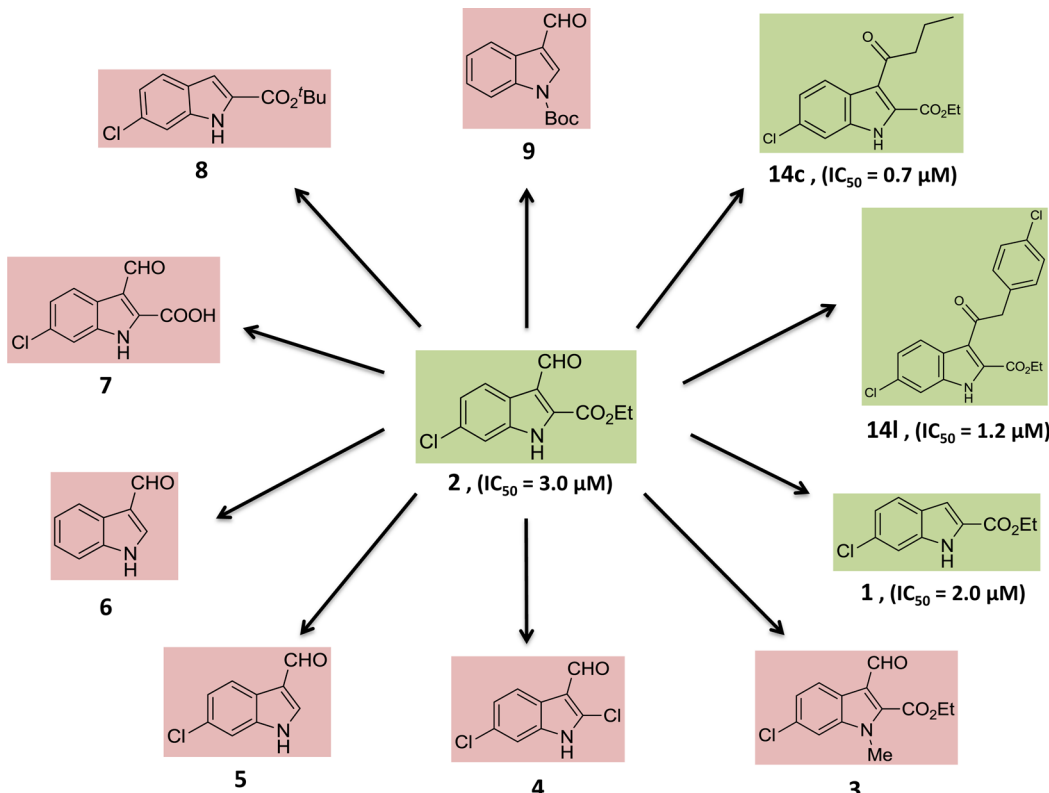


Figure 2. Substitution-oriented fragment screening (SOS) enables the identification of unique substitution patterns around known scaffolds, which can be further optimized by identification of structure–activity relationships (SAR) to support structure-based design.

in an early phase (Figure 1). Indole-based inhibitors, such as PD-146176 by Pfizer<sup>21</sup> and tryptamine sulfonamides by Bristol-Myers Squibb (BMS),<sup>22</sup> exhibited inhibitory potency against r12/15-LOX with  $\text{IC}_{50}$  values of  $3.81 \mu\text{M}$  and  $21 \text{ nM}$ , respectively. The inhibitor PD-146176 also showed down-regulation of interleukin-12 (IL-12) after its expression was stimulated with LPS.<sup>15</sup> However, the inhibitory potency of the PD-146176 is relatively low. Furthermore, five-membered heterocycles like pyrazole-based sulfonamides and sulfamides

( $\text{IC}_{50} = 1.4 \text{ nM}$ , r12/15-LOX) have been reported.<sup>23</sup> Also, oxadiazole or oxazole derivatives such as ML094 ( $\text{IC}_{50} = 10 \text{ nM}$ , h-15-LOX-1)<sup>24</sup> and ML351 ( $\text{IC}_{50} = 200 \text{ nM}$ , h-15-LOX-1)<sup>25</sup> are highly potent. Another class of potent h-15-LOX-1 inhibitors is imidazole-based ( $\text{IC}_{50} = 75 \text{ nM}$ , r12/15-LOX).<sup>26</sup> Less potent 15-LOX inhibitors are indolizine ( $\text{IC}_{50} = 25 \mu\text{M}$ , r12/15-LOX),<sup>27</sup> thiourea ( $\text{IC}_{50} = 1.8 \mu\text{M}$ , soybean 15-LOX),<sup>28</sup> and thiadiazine ( $\text{IC}_{50} = 9 \mu\text{M}$ , soybean 15-LOX)<sup>29</sup> derivatives. Recently, anacardic acid-derived salicylates were described by



**Figure 3.** Structure–activity relationship study of compound 2. Compounds with a red background do not inhibit h-15-LOX-1 at concentrations below 50  $\mu$ M, whereas compounds with a green background are active at inhibiting h-15-LOX-1 in the low micromolar range.

our research group as LOX inhibitors.<sup>30–32</sup> Although the potency of these inhibitors is moderate or good, they often suffer from unfavorable physicochemical properties<sup>33</sup> and limited ligand efficiency values (LE), which limit their utility as drug candidates. Taking into account all of the above, new chemotypes are needed in order to explore the structure–activity relationships (SAR) and the drugability of this enzyme further.

Currently available inhibitors are frequently built around nitrogen-containing heterocycles such as indoles, imidazoles, or pyrazoles. We anticipate that identifying the right substitution pattern is more demanding than finding a scaffold that provides inhibition. We therefore developed an approach for screening of fragments that is focused on specific nitrogen-containing heterocycles, such as indoles, quinolones, pyrazoles, and others, that have a very diverse substitution pattern. We denoted this approach substitution-oriented fragment screening (SOS). After having identified fragment hits with the right substitution pattern that give inhibition of h-15-LOX-1 in the micromolar range, we assumed that the active hits are sufficiently potent to provide initial SAR data. This will enable docking studies and structure-based design to optimize the substitution pattern further.

Here, we set out to test the SOS approach for fragment-based screening to find substituted scaffolds that inhibit the enzyme h-15-LOX-1 at micromolar concentrations. The hits were used to establish an initial SAR, and docking studies were performed to enable the proposal of a plausible binding mode for the new hits in line with the SAR. The hits were further optimized using structure-based design to yield inhibitors with potencies in the nanomolar range. The effects of the most potent inhibitor on pro- and anti-inflammatory gene expression

were investigated in RAW 264.7 macrophages and precision-cut lung slices (PCLS) of mouse lung tissue.

## ■ RESULTS AND DISCUSSION

### Initial Screening and Discovery of Potent Inhibitors.

For our SOS approach, we employed a library of 200 fragments containing 26 indoles, 73 quinolones, 22 pyrroles, and 79 other heterocycles with a diverse substitution pattern (Figure 2). This library consists mostly of di- or trisubstituted scaffolds with substituents varying among EWG, EDG, aliphatic, and aromatic moieties.

For h-15-LOX-1 activity studies, an assay was used that employs the UV absorption of the h-15-LOX-1 product ( $\lambda_{\text{max}}$  234 nm) formed upon enzymatic conversion from linoleic acid (Figure S1). This assay was done in a 96-well format, which is suited for medium-throughput screening, measurement of 50% inhibition concentrations (IC<sub>50</sub>), and enzyme kinetics studies. Using this assay, the SOS library was screened, and four hits were identified that provide more than 80% inhibition of the enzyme's activity at 50  $\mu$ M, which indicates an inhibitory potency in the low micromolar range. The potency was confirmed by determination of the IC<sub>50</sub> values for compounds 1 and 2 (Figure 3). The identified hits contain an indole scaffold, as has been previously found in h-15-LOX-1 inhibitors such as, for example, PD-146176 or tryptamine sulfonamides (Figure 1). Interestingly, the hits 6-chloro-1*H*-indole-2-ethyl acetate (1) and 6-chloro-3-formyl-1*H*-indole-2-ethyl acetate (2) both have a unique substitution pattern around the indole scaffold that has not been identified previously. Hits 1 and 2 have beneficial properties for further development because halogen substitution at the 5- or 6-position could prevent hydroxylation of the indole, thereby increasing its metabolic stability.<sup>34,35</sup> This

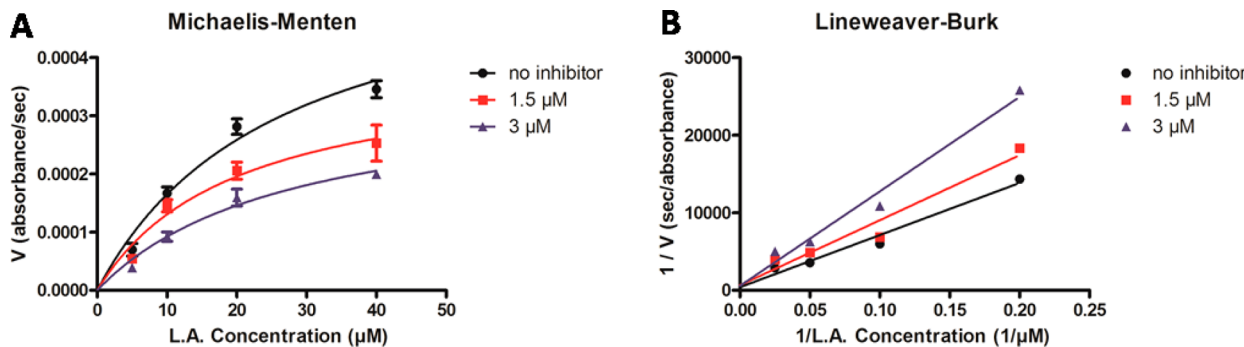


**Figure 4.** Steady-state kinetic characterization of h-15-LOX-1 in the presence of different concentrations of compound **14l**: (A) Michaelis–Menten representation and (B) Lineweaver–Burk representation.

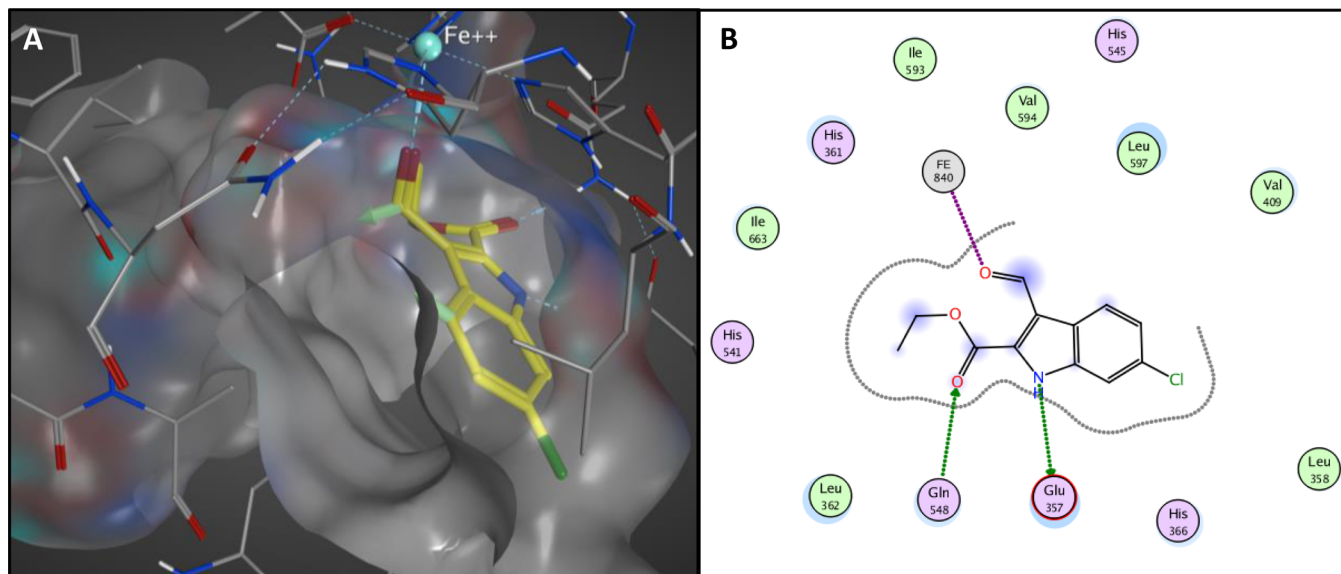


**Figure 5.** (A) Binding orientation of inhibitor **2** in the active site of h-15-LOX-1 proposed by molecular modeling studies. The surface of the active site of the enzyme is presented in gray, and the light green vectors in the compound show directions for possible extensions of the molecule. (B) 2D representation of the interactions of compound **2** with the active site of the enzyme.

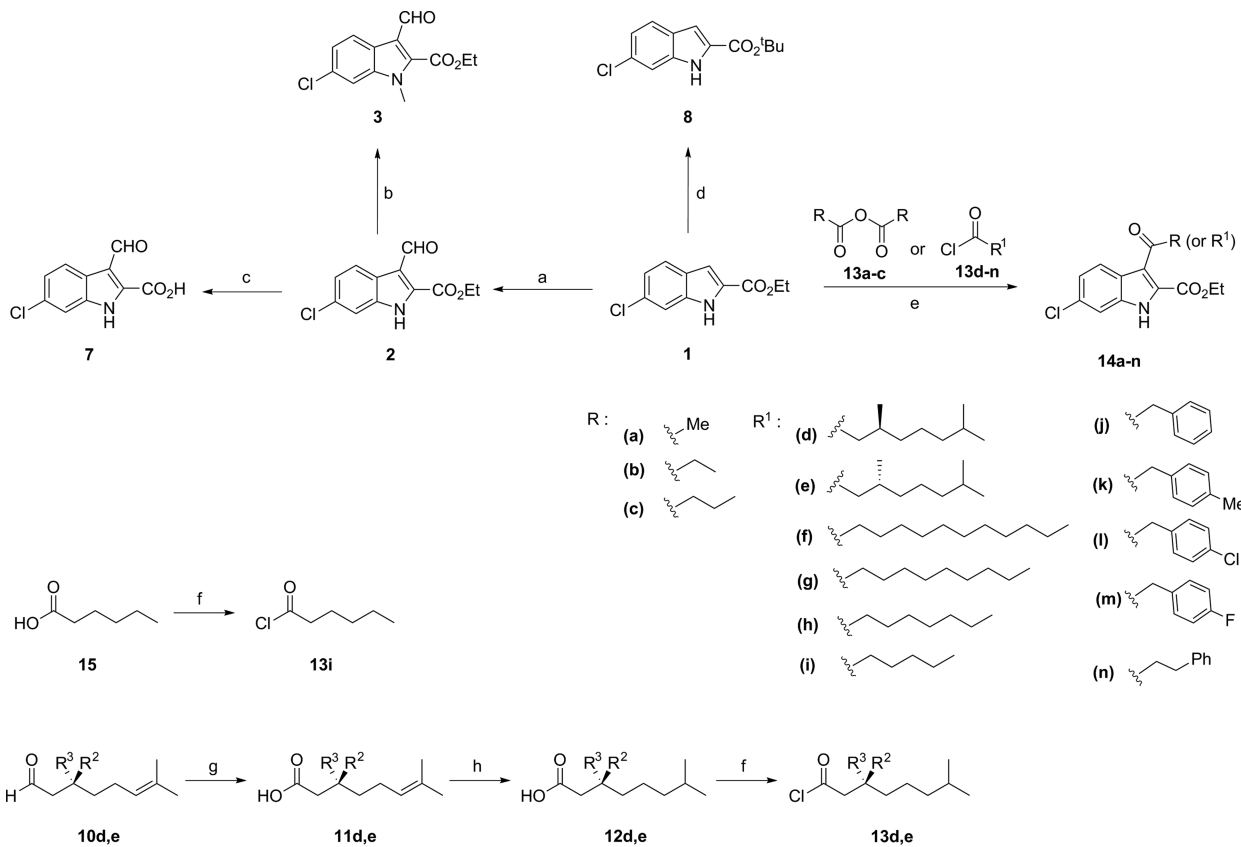
stresses the utility of the SOS approach to identify novel substitution patterns around known scaffolds.

An initial SAR was derived by comparison of **1** and **2** with a selection of compounds that have a closely related structure (Figure 3). We investigated the importance of the indole NH as a potential hydrogen-bond donor by methylation using MeI/K<sub>2</sub>CO<sub>3</sub> to give compound **3**, which inhibits the enzyme's activity by less than 50% at 50 μM. This indicates that the free NH is important for binding, possibly due to hydrogen-bond formation. Importantly, compounds **4**, **5**, **7**, and **8** are also inactive, which indicates that carboxy ethyl substitution in the 2-position is important for binding to the enzyme.

Comparison of **1** and **2** indicates that the 3-formyl substitution does not greatly change the inhibitory potency, thus indicating that larger substituents could be linked to this position. This suggestion is in line with literature on related indole-based inhibitors where substitution of the indole heterocycle at the 3-position markedly improved the h-15-LOX-1 inhibitory potency, as observed for inhibitors like PD-146176 or tryptamine sulfonamides (Figure 1). This led us to synthesize compounds **14c** and **14l** that are elongated at the 3-position. Compounds **14c** and **14l** were synthesized after acylation of 6-chloro-1*H*-indole-2-ethyl acetate (**1**) with butyric anhydride and 4-chlorophenylacetyl chloride, respectively, via a

Friedel–Crafts type reaction.<sup>36</sup> The IC<sub>50</sub> values were calculated to be  $0.7 \pm 0.3 \mu\text{M}$  for **14c** and  $1.2 \pm 0.5 \mu\text{M}$  for **14l**, which indicates a 2- to 2.5-fold improved inhibitory potency, probably due to lipophilic interactions. The fact that these inhibitors are more potent than compounds **1** and **2** indicates that substitution at this position is possible and could improve the potency of this type of inhibitor. To conclude, we confirmed that both the -NH and -ethyl acetate groups are playing a vital role in the inhibition of h-15-LOX-1 and that attachment of extended substitutions at the 3-position is possible with retention or even improvement of affinity. Having established this qualitative SAR, we performed molecular modeling studies and structure-based design in order to provide a rationale for our findings and to optimize the substitution in the 3-position.

In order to establish the mechanism of h-15-LOX-1 inhibition, Michaelis–Menten enzyme kinetics analysis in the presence of inhibitor **14l** was performed (Figure 4A,B). The Lineweaver–Burk double reciprocal plot shows that inhibitor **14l** causes an increase in the K<sub>m</sub> values, whereas the V<sub>max</sub> values remain more constant (Table S3), indicating competitive inhibition. Using the Cheng–Prusoff equation, the binding affinities (K<sub>i</sub>) of all of the inhibitors were calculated and are shown in Table 1.

Scheme 1. General Synthesis<sup>a</sup>

d: R<sup>2</sup> = Me and R<sup>3</sup> = H, e: R<sup>2</sup> = H and R<sup>3</sup> = Me

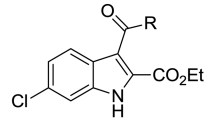
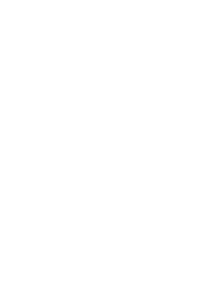
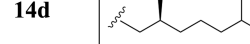
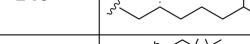
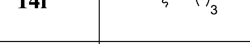
<sup>a</sup>Reagents and conditions: (a) POCl<sub>3</sub>, DMF, 60 °C, overnight; (b) K<sub>2</sub>CO<sub>3</sub>, CH<sub>3</sub>I, acetone, rt, 2 h; (c) LiOH, EtOH/H<sub>2</sub>O, rt, 24 h; (d) H<sub>2</sub>SO<sub>4</sub>, MgSO<sub>4</sub>, DCM, 'BuOH, rt, overnight; (e) SnCl<sub>4</sub>, CH<sub>3</sub>NO<sub>2</sub>, DCM, rt, overnight; (f) (COCl)<sub>2</sub>, DCM, 0 °C for 30 min and then rt for 3 h; (g) Ag<sub>2</sub>O, H<sub>2</sub>O, rt, overnight; (h) H<sub>2</sub>, Pd/C, EtOH, 40 °C, overnight.

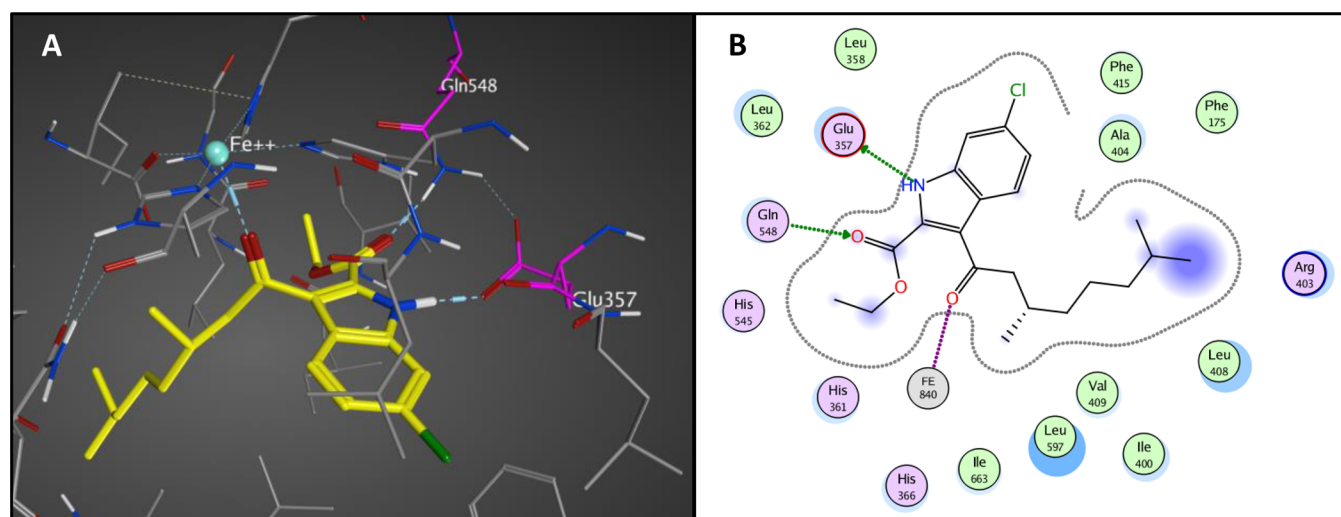
In order to link the observed SAR to structural information, compound 2 was docked in the active site of the enzyme in line with the identified competitive inhibition. Due to the fact that there is no crystal structure of human 15-LOX-1 available, the docking study was performed with the crystal structure of rabbit 15-LOX (PDB: ILOX), as determined by Gillmor et al.<sup>37</sup> This is justified by the high sequence similarity (87%) between rabbit 15-LOX and human 15-LOX-1, with the main differences between them being located in the N-terminal domain and not in the catalytic domain. In three of the top five highest scoring poses, inhibitor 2 binds in the same orientation in the active site of the enzyme, forming a hydrogen bond with Glu357 (Figure S4). Subsequent energy minimization in the active site provided the final binding model for inhibitor 2 (Figure 5). The modeling shows the presence of two hydrogen bonds: the first is between Gln548 and the 2-carboxy ethyl group and the second is between the -NH group and Glu357 (Figure 5B). The formyl group in the 3-position results in an interaction with iron in the enzyme, and there is space to extend the substitution in this position due to the presence of free space in the substrate binding pocket (Figure 5A). The 2-carboxy ethyl of inhibitor 2 is tightly embedded in the binding pocket, which is in line with the lack of inhibition observed for 2-carboxy tertbutyl-substituted compound 8 (Figure 3). The features in this model are consistent with the observed SAR, thus justifying

the application of this model as a basis for structure-based design to optimize the substituent at the 3-position.

**Structure-Based Design.** Our SAR-based model indicates that optimization of the inhibitor by acylation in the indole 3-position is feasible. The free space in the enzyme binding pocket that should be addressed this way mainly has hydrophobic character, in line with the character required for binding to its natural substrate, linoleic acid. Taking this into account, we synthesized a library of 14 derivatives to explore the SAR for substitution at this position. Exclusive acylation on the 3-position of inhibitor 1 as starting material was achieved using a Friedel-Crafts-type acylation with different acid chlorides or anhydrides. The reactions were performed in the presence of SnCl<sub>4</sub> and CH<sub>3</sub>NO<sub>2</sub> in DCM, yielding the corresponding compounds, 14a–n, in good to excellent yields (Scheme 1). All of the compounds were analytically pure after simple washing steps, underscoring the facile nature of their synthetic preparation. The acid chlorides, which are not commercially available, were synthesized from the corresponding acids using oxalyl chloride in DCM in quantitative yields and used without further purification. Enantiomerically pure products 14d,e were prepared in a four-step reaction sequence starting from commercially available (R)-(+) or (S)-(−)-citronellal. Initially, aldehydes 10d,e were oxidized to carboxylic acids 11d,e using Tollens' reagent, and the double bonds were reduced with Pd/C under a H<sub>2</sub> atmosphere to give 12d,e. Next,

Table 1. Collection of the Synthesized Inhibitors with  $IC_{50}$  and  $K_i$  Values

	Compound	R	$IC_{50}$ value ( $\mu M$ )	$K_i$ value ( $\mu M$ )
	<b>14a</b>		$2.31 \pm 0.71$	$0.93 \pm 0.28$
	<b>14b</b>		$1.78 \pm 0.27$	$0.72 \pm 0.10$
	<b>14c</b>		$0.73 \pm 0.29$	$0.29 \pm 0.12$
	<b>14d</b>		$0.09 \pm 0.03$	$0.03 \pm 0.01$
	<b>14e</b>		$0.30 \pm 0.15$	$0.12 \pm 0.06$
	<b>14f</b>		$0.43 \pm 0.27$	$0.17 \pm 0.10$
	<b>14g</b>		$0.20 \pm 0.07$	$0.08 \pm 0.03$
	<b>14h</b>		$0.27 \pm 0.10$	$0.10 \pm 0.04$
	<b>14i</b>		$0.54 \pm 0.30$	$0.21 \pm 0.12$
	<b>14j</b>		$0.60 \pm 0.31$	$0.25 \pm 0.12$
	<b>14k</b>		$2.08 \pm 1.33$	$0.83 \pm 0.53$
	<b>14l</b>		$1.19 \pm 0.48$	$0.48 \pm 0.19$
	<b>14m</b>		$0.77 \pm 0.30$	$0.31 \pm 0.12$
	<b>14n</b>		$0.56 \pm 0.28$	$0.22 \pm 0.11$

Figure 6. (A) Binding of compound **14d** in the active site of 15-LOX-1 after molecular modeling studies. (B) 2D illustration of the interactions of compound **14d** with the active site of the enzyme.

acid chlorides **13d,e** were synthesized and coupled with the 6-chloro-1*H*-indole-2-ethyl acetate (**1**), resulting in desired products **14d,e** (Scheme 1).

All of the newly synthesized compounds were subjected to  $IC_{50}$  determination in a h-15-LOX-1 inhibition assay, and the values are shown in Table 1. We first explored inhibitors with a phenyl group in the 3-substituent in which we varied both the position of the phenyl group and the electronic and steric

properties (**14j–n**). However, changing the phenyl substitution in **14j** to **14m**, **14l**, and **14k** did not improve the inhibition. Also, changing the position of the phenyl group in **14j** to **14n** did not greatly affect the inhibition, although the potency at  $0.56 \mu M$  is reasonably good. We then explored another route of optimization with compounds **14a–i**, in which the length of the lipophilic tail is varied from 1 to 11 carbon atoms. This series of inhibitors showed a clear SAR, with optimal binding

demonstrated for **14g** having 9 aliphatic carbons in the lipophilic tail. The clear activity dependence on the length of the aliphatic tail, from 2.3 to 0.4  $\mu\text{M}$  (Table 1), indicates the role for lipophilic interactions in the binding, which is in accord with the molecular modeling study. The successful optimization of the inhibitors with an aliphatic acylation in the 3-position triggered our interest in including an aliphatic tail that was identified in a previous study,<sup>32</sup> as reflected in inhibitors **14d,e**. Previously, we found that an aliphatic tail that branches at the 3,7-position improves the inhibitory activity for h-15-LOX-1.<sup>32</sup> We included these structural features in our inhibitors as a further optimization of the aliphatic substituent at the 3-position. The resulting inhibitors, **14e** and **14d**, contain a stereogenic center, and the stereochemistry (*R* or *S*) affected the affinity by a 3-fold difference in potency. The *S* enantiomer (**14d**) provided the highest potency, thus reaching an  $\text{IC}_{50}$  value of  $0.09 \pm 0.03 \mu\text{M}$ , which reflects a  $K_i$  value of  $0.03 \pm 0.01 \mu\text{M}$ .

Molecular modeling of inhibitor **14d** in the active site of the enzyme using procedures applied for inhibitor **2** provided a binding configuration in which the 6-chloro-1*H*-indole-2-ethyl acetate moiety binds in a manner similar to the docking of inhibitor **2**. The extension of the substituent in the 3-position fills the lipophilic binding pocket available in this position. The docking again shows the presence of two hydrogen bonds with Gln548 and Glu357 and the interaction with iron, and the branched aliphatic tail occupies the lipophilic binding pocket completely (Figures 6 and S5). This SAR is in total agreement with the observed activity data in which **14g** is the most potent inhibitor with a linear aliphatic tail and **14d** reaches the highest affinity with a branched aliphatic tail.

**Ligand Efficiency Metrics.** The SOS-based development strategy provided **14d** as an inhibitor with nanomolar potency that can be further investigated in biochemical studies. To support development of inhibitors from this stage toward successful application in drug discovery projects, they need to show acceptable physicochemical properties to achieve an acceptable ADME-Tox (absorption, distribution, metabolism, excretion, and toxicity) profile *in vivo*. To this end, ligand efficiency metrics have been rendered into a generally accepted tool to estimate the value of lead compounds.<sup>38</sup> Therefore, ligand efficiency metrics and indices such as ligand efficiency (LE), binding efficiency index (BEI), and surface efficiency index (SEI) were calculated for **14d** in comparison to those of previously described inhibitors (Table 2). Ligand efficiency is defined as the binding affinity of a ligand in relation to the number of non-hydrogen atoms (HA) according to the equation  $\text{LE} = (1.37/\text{HA}) \times \text{p}K_i$ .<sup>39</sup> Inhibitor **14d** has 26

heavy atoms (non-hydrogen), and the  $K_i$  value is  $0.03 \mu\text{M}$ , so the LE is equal to  $0.40 \text{ kcal/mol per HA}$ . LE values  $>0.3 \text{ kcal/mol}$  are considered to be acceptable LE values for drug candidates.<sup>40</sup> Inhibitor **14d** satisfies the requirements and exceeds the values calculated for previously described inhibitors except for inhibitor PD-146176. Another parameter is BEI, which is the binding efficiency index that relates potency to molecular weight on a per kilodalton scale, and SEI is the surface efficiency index, which monitors the gains in potency related to the increase in polar surface area (PSA) referenced to  $100 \text{ \AA}^2$ .<sup>41</sup> BEI and the SEI for **14d** and the other inhibitors were calculated according to the equations  $\text{BEI} = \text{p}K_i/\text{MW}$  and  $\text{SEI} = \text{p}K_i/(\text{PSA}/100 \text{ \AA}^2)$ .<sup>41</sup> The MW of inhibitor **14d** is  $377 \text{ Da}$  or  $0.377 \text{ kDa}$ , so the BEI is 19.90. The PSA was estimated from MarvinSketch software to be  $59.16 \text{ \AA}^2$ , and on the basis of this PSA, the SEI for compound **14d** is 12.71. Reference values for these parameters were obtained from mapping the surface binding and binding efficiency indices (SEI–BEI values) for 92 examples of marketed drugs, which provided average values for SEI of  $17.9 \pm 15.7$  and BEI of  $28.0 \pm 11.5$ .<sup>38</sup> The parameters for inhibitor **14d** lay well with this range (Table 2). In addition, we calculated the lipophilic ligand efficiency (LLE) to estimate the balance between affinity and lipophilicity.<sup>40</sup> The LLE for **14d** has a value comparable to that of other compounds except for the pyrazole-based sulfamide and ML094, which show more favorable values. This indicates that **14d** can be improved with respect to its lipophilicity. In conclusion, the ligand efficiency metrics for **14d** demonstrate its favorable binding efficiency compared to that of previously described inhibitors, which justifies further investigation of this molecule in biochemical studies.

**Gene Expression Profiling.** Having identified **14d** as a potent inhibitor for h-15-LOX-1, we moved on to study its effects in model systems for inflammatory lung diseases using *in vitro* studies with RAW 264.7 macrophages and *ex vivo* studies with precision-cut lung slices (PCLS). As a first step, the cytotoxicity of compound **14d** was investigated in RAW 264.7 cells as well as in PCLS in order to identify the concentration range at which this inhibitor does not affect cell viability. Inhibitor **14d** did not inhibit cell viability at concentrations below  $12.5 \mu\text{M}$  in RAW 264.7 cells (Figure 7A), as determined using an MTS assay. The viability of PCLS was determined by measuring the release of lactate dehydrogenase (LDH) into the medium upon incubation with different concentrations of inhibitor **14d**. LDH release demonstrated that inhibitor **14d** does not affect PCLS viability at concentrations of  $500 \text{ nM}$  and lower (Figure 7B).

Having identified the nontoxic concentration for inhibitor **14d**, its influence on gene expression was investigated. In these models, LPS/INF $\gamma$  was applied as an inflammatory stimulus, and the influence of **14d** on the expression of pro-inflammatory genes IL-1 $\beta$ , IL-6, or IL-12 and the anti-inflammatory gene IL-10 was investigated. Since the cellular concentration of free fatty acids (the preferred substrate of mammalian LOXs) is rather low, we supplemented the culture medium with linoleic acid (C18: $\Delta 2$ ,  $n = 6$ ), which is the most abundant polyenoic fatty acid in mammalian cells and serves as a natural substrate for 15-LOX-1. Linoleic acid itself did not alter the expression of IL-1 $\beta$ , IL-6, IL-10, and IL-12 in RAW 264.7 cells and PCLS (data not shown).

In LPS/INF $\gamma$ -stimulated RAW 264.7 macrophages, incubation with h-15-LOX-1 inhibitor **14d** did not change the expression of the genes encoding IL-1 $\beta$ , IL-6, and IL-12, but it

**Table 2. Binding Affinity and Ligand Efficiency Metrics and Indices<sup>38,40</sup> of Previously Published 15-LOX-1 Inhibitors (Shown in Figure 1) and Newly Synthesized Inhibitor **14d****

15-LOX inhibitors	$K_i$ ( $\mu\text{M}$ )	LE <sup>a</sup>	BEI	SEI	LLE
<b>14d</b>	0.036	0.40	19.90	12.71	0.6
PD-146176	3.81	0.43	22.79	34.31	1.0
tryptamine sulfonamide	0.021	0.30	15.71	10.78	-0.5
pyrazole-based sulfamide	0.001	0.32	15.54	8.26	4.9
imidazole-based sulfamide	0.073	0.24	11.93	7.88	0.9
ML094	0.010	0.36	19.12	12.26	3
indolizine	25.0	0.19	10.47	9.63	-2

<sup>a</sup>The units for LE are (kcal/mol·HA)

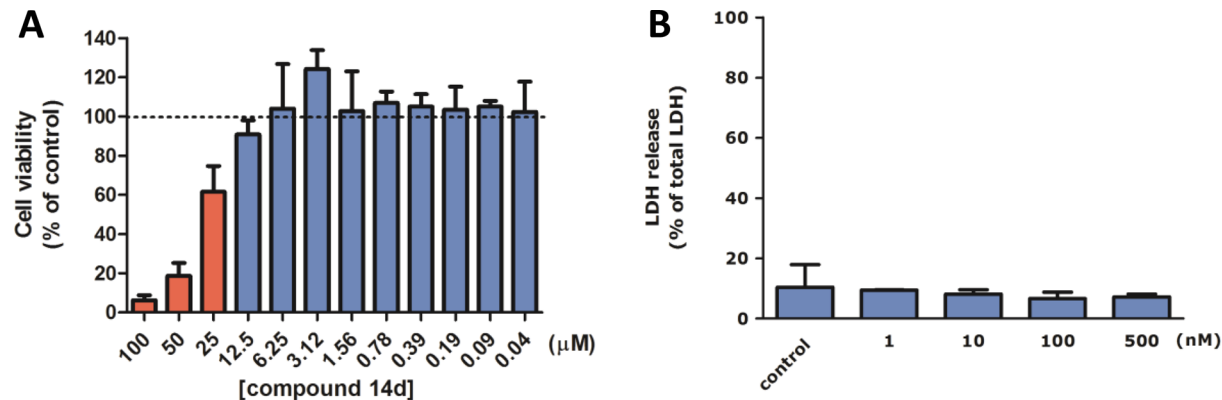


**Figure 7.** (A) LC<sub>50</sub> graph after MTS assay. Compound **14d** was incubated with RAW 264.7 cells at concentrations from 0.04 to 100  $\mu\text{M}$ . Red bars are statistically different compared to nontreated control cells. (B) Viability of precision-cut lung slices (PCLS) measured by release of lactate dehydrogenase (LDH) into the incubation medium. PCLS were treated with various concentrations of **14d** (1, 10, 100, and 500 nM) and 10  $\mu\text{M}$  linoleic acid for 20 h. Maximal LDH content of the PCLS was determined by lysis with 1% Triton X-100. LDH release was plotted relative to maximal LDH. Data are presented as mean values  $\pm$  SD of three independent experiments.

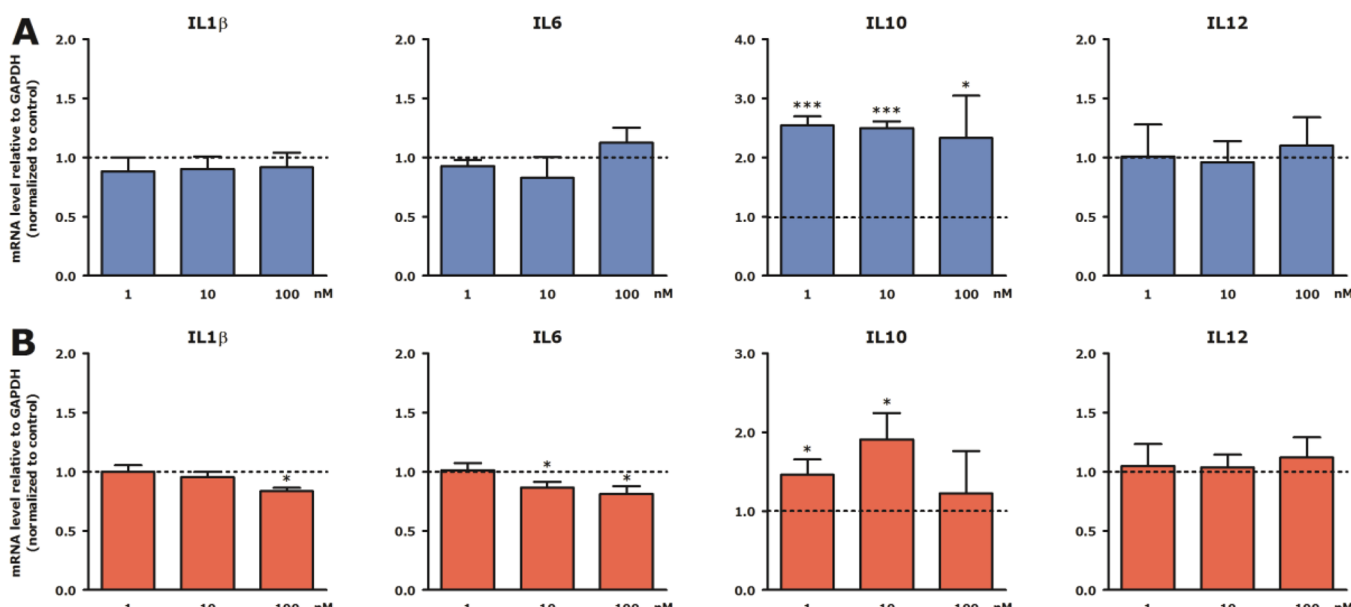


**Figure 8.** Effect of h-15-LOX-1 inhibition on interleukin expression in RAW 264.7 cells and precision-cut lung slices (PCLS). Stimulated RAW 264.7 cells (A) and PCLS (B) were subjected to **14d** in combination with 10  $\mu\text{M}$  linoleic acid for 20 h and stimulated with LPS/IFN $\gamma$  for the last 4 h. Subsequently, RAW 264.7 cells and PCLS were lysed, and gene expression was assessed by RT-qPCR and expressed as fold change compared to control (LPS/IFN $\gamma$ /linoleic acid-treated) group. Data are presented as mean values  $\pm$  SEM of 4–6 independent experiments. \*  $p < 0.05$ ; \*\*\*  $p < 0.001$  compared to control.

provided a more than 2-fold increase in the expression of IL-10 at concentrations as low as 1 nM (Figure 8A). Since IL-10 has anti-inflammatory properties and is connected with the anti-inflammatory M2 macrophage phenotype, the observed changes in gene expression are indicative of a potential anti-inflammatory effect of **14d**. Next, the effect of **14d** on the expression of LPS/INF $\gamma$ -induced cytokines in PCLS was assessed. In line with the results obtained in macrophages, the expression of IL-10 is upregulated in PCLS. In addition, there is a small but significant downregulation of the pro-inflammatory genes IL-1 $\beta$  and IL-6 (Figure 8B). Remarkably, the expression of IL-12 remained unchanged, although others have reported that h-15-LOX-1 regulates the production of IL-12 in macrophages.<sup>15</sup> The induction of IL-10 in PCLS seems to show a bell-shaped pattern. This could mean that h-15-LOX-1 inhibition in this system is effective in a limited range of

concentrations, with 10 nM being the optimal dose. Nevertheless, further research is needed regarding this observation. The effect of **14d** on IL-10 expression is remarkable because the important role of IL-10 in inflammatory lung diseases has been previously highlighted in a study that showed diminished IL-10 production in lung tissue of COPD patients after LPS stimulation as compared to that in lung tissue of patients with normal lung function.<sup>42</sup> In addition, it has been demonstrated that the level of IL-10 and IL-10-positive macrophages in sputum of COPD patients and healthy smokers was decreased as compared to that in healthy nonsmokers.<sup>43</sup> This suggests that macrophages in COPD have lost their ability to produce anti-inflammatory cytokines like IL-10 and are therefore unable to effectively dampen inflammation. Our newly developed inhibitor **14b** could, among others, alleviate the lack of IL-10 production in these diseases. Nevertheless, we note that

overexpression of IL-10 can be associated with certain types of cancer,<sup>44</sup> which indicates that the final effect of this inhibitor in disease models needs to be evaluated carefully. Taken together, we demonstrate that the effects observed for treatment with inhibitor **14d** are in agreement with an anti-inflammatory effect that could be beneficial in inflammatory lung diseases. This sets the stage for further investigation and optimization of inhibitor **14d** for *in vivo* applications toward the development of novel therapeutics for inflammatory lung diseases.

## CONCLUSIONS

In this study, we employed an efficient strategy to identify structurally new inhibitors for the enzyme h-15-LOX-1, which is an emerging drug target in various inflammatory diseases. Our approach started with a substitution-oriented fragment screening (SOS) of a focused fragment library containing diversely substituted heterocycles. After the discovery of four hits, two inhibitors were selected to derive structure–activity relationships and subjected to enzyme kinetics analysis, which indicated competitive inhibition. These observations were applied to support a molecular modeling study that proposed a binding configuration in the active site of h-15-LOX-1. On the basis of this model, the substitution of the inhibitor was further optimized using structure-based design to provide inhibitor **14d** with a  $K_i$  of 36 nM and good ligand efficiency metrics. This inhibitor was evaluated in cell-based studies using RAW 264.7 macrophages and *ex vivo* studies in mouse precision-cut lung slices. The inhibitor provided an increase in the expression of IL-10 in both macrophages and mouse lung tissue. In the future, these inhibitors could be used as lead compounds for further optimization or as a starting point of drug discovery efforts targeting h-15-LOX-1.

## EXPERIMENTAL SECTION

**Chemistry. General.** The solvent and reagents were purchased from Sigma-Aldrich and Acros chemicals and were used without further purification unless otherwise noted. Reactions were monitored by thin-layer chromatography (TLC). Merck silica gel 60 F<sub>254</sub> plates were used, and spots were detected under UV light or after staining with potassium permanganate for non UV-active compounds. MP Ecochrom silica 32–63, 60 Å was used for flash column chromatography. <sup>1</sup>H NMR (500 MHz) and <sup>13</sup>C NMR (126 MHz) spectra were recorded with a Bruker Avance four-channel NMR spectrometer with a TXI probe. Chemical shifts were referenced to the residual proton and carbon signals of the deuterated solvent, CDCl<sub>3</sub>: δ = 7.26 ppm (<sup>1</sup>H) and 77.05 ppm (<sup>13</sup>C). The following abbreviations were used for spin multiplicity: s = singlet, br s = broad singlet, d = doublet, t = triplet, q = quartet, quin = quintet, dd = double of doublets, ddd = double of doublet of doublets, and m = multiplet. Fourier transform mass spectrometry (FTMS) and electrospray ionization (ESI) spectra were recorded on an Applied Biosystems/SCIEX API3000-triple quadrupole mass spectrometer. All compounds were analyzed with a Waters Investigator Semiprep 15 SFC-MS instrument, confirming their purity to be ≥95%. The corresponding chromatographs are shown in the Supporting Information.

**Synthetic Procedure 1: Indole 3-Acylation.** Indole (1.0 mmol) was dissolved in 4.0 mL of DCM under a nitrogen atmosphere, and the solution was cooled to 0 °C. To the stirring solution was added SnCl<sub>4</sub> (1.2 mmol) in a single portion via syringe. After the ice bath was removed, the mixture was stirred at room temperature for 30 min, and then the acyl chloride or anhydride (1.0 mmol) was added in small portions, followed by the addition of nitromethane (3.0 mL). The reaction mixture was stirred at room temperature overnight. After being quenched with cold water (10 mL), the organic material was extracted with EtOAc (2 × 15 mL), dried over MgSO<sub>4</sub>, filtered, and concentrated under reduced pressure.

**Ethyl 3-acetyl-6-chloro-1H-indole-2-carboxylate (14a, DN397).** The final product was obtained after 3-acylation of indole **1** using synthetic procedure 1. Pink solid, yield 75%. <sup>1</sup>H NMR (500 MHz, CDCl<sub>3</sub>) δ 9.28 (br s, 1H), 8.00 (d, *J* = 10.0 Hz, 1H), 7.41 (d, *J* = 0.5 Hz, 1H), 7.22 (dd, *J* = 8.7, 1.7 Hz, 1H), 4.48 (q, *J* = 7.2 Hz, 2H), 2.75 (s, 3H), 1.45 (t, *J* = 7.2 Hz, 3H). <sup>13</sup>C NMR (126 MHz, CDCl<sub>3</sub>) δ 198.3, 160.8, 135.4, 132.3, 127.3, 125.4, 124.0, 123.9, 121.7, 111.8, 62.5, 32.1, 14.3. MS (ESI): *m/z* 264.0 [M – H]<sup>+</sup>.

**Ethyl 6-Chloro-3-propionyl-1H-indole-2-carboxylate (14b, N239).** The final product was obtained after 3-acylation of indole **1** using synthetic procedure 1. Orange solid, yield 82%. <sup>1</sup>H NMR (500 MHz, CDCl<sub>3</sub>) δ 9.17 (s, 1H), 7.86 (d, *J* = 8.7 Hz, 1H), 7.41 (d, *J* = 1.6 Hz, 1H), 7.20 (dd, *J* = 8.7, 1.6 Hz, 1H), 4.45 (q, *J* = 7.1 Hz, 2H), 3.08 (q, *J* = 7.3 Hz, 2H), 1.43 (t, *J* = 7.1 Hz, 3H), 1.23 (t, *J* = 7.3 Hz, 3H). <sup>13</sup>C NMR (126 MHz, CDCl<sub>3</sub>) δ 201.7, 160.6, 135.3, 132.3, 126.1, 125.2, 123.7, 123.6, 121.9, 111.5, 62.1, 37.3, 14.2, 8.6. MS (ESI): *m/z* 302.1 [M + Na]<sup>+</sup>.

**Ethyl 3-Butyryl-6-chloro-1H-indole-2-carboxylate (14c, N238).** The final product was obtained after 3-acylation of indole **1** using synthetic procedure 1. Orange solid, yield 83%. <sup>1</sup>H NMR (500 MHz, CDCl<sub>3</sub>) δ 9.16 (s, 1H), 7.85 (d, *J* = 8.7 Hz, 1H), 7.41 (d, *J* = 1.8 Hz, 1H), 7.20 (dd, *J* = 8.7, 1.8 Hz, 1H), 4.46 (q, *J* = 7.1 Hz, 2H), 3.04 (t, *J* = 7.4 Hz, 2H), 1.76 (m, 2H), 1.43 (t, *J* = 7.1 Hz, 3H), 0.98 (t, *J* = 7.4 Hz, 3H). <sup>13</sup>C NMR (126 MHz, CDCl<sub>3</sub>) δ 201.3, 160.6, 135.2, 132.2, 126.1, 125.2, 123.6, 123.5, 122.2, 111.5, 62.1, 46.1, 18.2, 14.3, 13.9. MS (ESI): *m/z* 316.1 [M + Na]<sup>+</sup>.

**Synthetic Procedure 2: Oxidation with Tollens' Reagent.** Fresh silver oxide was prepared by dropwise addition of a solution of AgNO<sub>3</sub> (2.3 mmol) in water (4.0 mL) to a stirred solution of NaOH (4.9 mmol) in water (4.0 mL) at 0 °C and further stirring for 30 min in the dark while a brown precipitate formed. Under continuous stirring, the aldehyde (1.0 mmol) was added dropwise, and the reaction was stirred overnight. The resulting suspension was filtered and washed with hot water (2 × 10 mL), and the clear solution was acidified with aqueous HCl (4N) to pH < 1. The solution was extracted with Et<sub>2</sub>O (3 × 20 mL), dried over MgSO<sub>4</sub>, filtered, and concentrated under reduced pressure.

**Synthetic Procedure 3: Reduction of the Alkene.** The alkene (1.0 mmol) and Pd/C (10%) (0.10 mmol) were suspended in EtOH (10 mL). The suspension was stirred under a H<sub>2</sub> atmosphere at 40 °C overnight. Subsequently, the mixture was filtered through Celite, and after that, the solvent was evaporated under reduced pressure.

**Synthetic Procedure 4: Conversion of Carboxylic Acids to Acid Chlorides.** The acid was dissolved in dry DCM (5.0 mL) under a nitrogen atmosphere, and the solution was cooled to 0 °C. A solution of oxalyl chloride (1.2 mmol) in dry DCM (4.0 mL) was added dropwise, and the solution was stirred under a nitrogen atmosphere at room temperature for an additional 3 h. The solvent and the excess of oxalyl chloride were evaporated under reduced pressure, yielding the product as a yellow oil.

**(S)-3,7-Dimethyloct-6-enoic Acid (11d, N240).** The final product was obtained after oxidation of (S)-3,7-dimethyloct-6-enal with Tollens' reagent using synthetic procedure 2. Yellow oil, yield 94%. <sup>1</sup>H NMR (500 MHz, CDCl<sub>3</sub>) δ 10.40 (s, 1H), 5.08 (t, *J* = 7.1 Hz, 1H), 2.35 (dd, *J* = 15.0, 5.8 Hz, 1H), 2.14 (dd, *J* = 15.0, 8.3 Hz, 1H), 2.07–1.92 (m, 3H), 1.67 (s, 3H), 1.59 (s, 3H), 1.37 (m, 1H), 1.24 (m, 1H), 0.97 (d, *J* = 6.7 Hz, 3H). <sup>13</sup>C NMR (126 MHz, CDCl<sub>3</sub>) δ 179.9, 131.6, 124.2, 41.6, 36.7, 29.8, 25.7, 25.4, 19.6, 17.6.

**(S)-3,7-Dimethyloctanoic Acid (12d, N242).** The final product was obtained after reduction of the alkene of (S)-3,7-dimethyloct-6-enoic acid using synthetic procedure 3. Yellow oil, quantitative yield. <sup>1</sup>H NMR (500 MHz, CDCl<sub>3</sub>) δ 10.68 (s, 1H), 2.33 (dd, *J* = 15.0, 5.9 Hz, 1H), 2.13 (dd, *J* = 15.0, 8.2 Hz, 1H), 1.95 (m, 1H), 1.51 (m, 1H), 1.34–1.12 (m, 6H), 0.95 (d, *J* = 6.8 Hz, 3H), 0.85 (d, *J* = 7.0 Hz, 6H). <sup>13</sup>C NMR (126 MHz, CDCl<sub>3</sub>) δ 180.0, 41.7, 39.0, 36.9, 30.2, 27.9, 24.7, 22.7, 22.6, 19.7.

**(R)- or (S)-Ethyl 6-Chloro-3-(3,7-dimethyloctanoyl)-1H-indole-2-carboxylate (14e (N246), 14d (N247)).** The final product was obtained after 3-acylation of indole **1** using synthetic procedure 1. White solid, yield 89%. <sup>1</sup>H NMR (500 MHz, CDCl<sub>3</sub>) δ 9.20 (s, 1H),

7.84 (d,  $J = 8.7$  Hz, 1H), 7.41 (s, 1H), 7.20 (d,  $J = 8.7$  Hz, 1H), 4.55 (q,  $J = 7.1$  Hz, 2H), 3.09 (dd,  $J = 15.8, 5.7$  Hz, 1H), 2.88 (dd,  $J = 15.8, 8.2$  Hz, 1H), 2.11 (m, 1H), 1.43 (t,  $J = 7.1$  Hz, 3H), 1.35–1.06 (m, 7H), 0.94 (d,  $J = 6.7$  Hz, 3H), 0.83 (d,  $J = 6.7$  Hz, 6H).  $^{13}\text{C}$  NMR (126 MHz,  $\text{CDCl}_3$ )  $\delta$  201.3, 160.6, 135.3, 132.2, 126.0, 125.2, 123.6, 123.5, 122.5, 111.6, 62.1, 51.6, 39.1, 37.3, 30.4, 27.9, 24.8, 22.7, 22.6, 20.0, 14.3. MS (ESI):  $m/z$  400.2 [M + Na]<sup>+</sup>.

**Ethyl 6-Chloro-3-dodecanoyl-1*H*-indole-2-carboxylate (14f, DN433).** The final product was obtained after 3-acylation of indole 1 using synthetic procedure 1. Red solid, yield 91%.  $^1\text{H}$  NMR (500 MHz,  $\text{CDCl}_3$ )  $\delta$  9.28 (br s, 1H), 7.84 (d,  $J = 8.7$  Hz, 1H), 7.41 (d,  $J = 1.8$  Hz, 1H), 7.20 (dd,  $J = 8.7, 1.8$  Hz, 1H), 4.46 (q,  $J = 7.1$  Hz, 2H), 3.06 (t,  $J = 7.6$  Hz, 2H), 1.75–1.71 (m, 2H), 1.36 (t,  $J = 7.1$  Hz, 3H), 1.33–1.24 (m, 16H), 0.89–0.86 (m, 3H).  $^{13}\text{C}$  NMR (126 MHz,  $\text{CDCl}_3$ )  $\delta$  201.7, 160.9, 135.5, 132.4, 126.2, 125.4, (2 $\times$ ) 123.7, 122.4, 111.7, 62.3, 44.5, 32.1, 29.8, 29.7, 29.5, 24.9, 22.9, 14.4, 14.3. MS (ESI):  $m/z$  428.2 [M + Na]<sup>+</sup>.

**Ethyl 6-Chloro-3-decanoyl-1*H*-indole-2-carboxylate (14g, DN432).** The final product was obtained after 3-acylation of indole 1 using synthetic procedure 1. Red solid, yield 91%.  $^1\text{H}$  NMR (500 MHz,  $\text{CDCl}_3$ )  $\delta$  9.25 (br s, 1H), 7.84 (d,  $J = 8.7$  Hz, 1H), 7.41 (d,  $J = 1.8$  Hz, 1H), 7.21 (dd,  $J = 8.7, 1.8$  Hz, 1H), 4.45 (q,  $J = 7.2$  Hz, 2H), 3.05 (t,  $J = 7.5$  Hz, 2H), 1.74–1.71 (m, 2H), 1.43 (t,  $J = 7.2$  Hz, 3H), 1.33–1.24 (m, 14H), 0.87 (t,  $J = 7.1$  Hz, 3H).  $^{13}\text{C}$  NMR (126 MHz,  $\text{CDCl}_3$ )  $\delta$  201.7, 160.8, 135.5, 132.4, 126.2, 125.4, 123.8, 123.7, 122.4, 111.7, 62.3, 44.5, 32.1, 29.6, 29.6, 29.5, 29.4, 24.9, 22.9, 14.4, 14.3. MS (ESI):  $m/z$  400.2 [M + Na]<sup>+</sup>.

**Ethyl 6-Chloro-3-octanoyl-1*H*-indole-2-carboxylate (14h, N214).** The final product was obtained after 3-acylation of indole 1 using synthetic procedure 1. Orange solid, yield 93%.  $^1\text{H}$  NMR (500 MHz,  $\text{CDCl}_3$ )  $\delta$  9.25 (s, 1H), 7.84 (d,  $J = 8.7$  Hz, 1H), 7.40 (d,  $J = 1.8$  Hz, 1H), 7.19 (dd,  $J = 8.7, 1.8$  Hz, 1H), 4.45 (q,  $J = 7.2$  Hz, 2H), 3.05 (t,  $J = 7.5$  Hz, 2H), 1.74–1.68 (m, 2H), 1.43 (t,  $J = 7.2$  Hz, 3H), 1.37–1.23 (m, 8H), 0.86 (t,  $J = 6.7$  Hz, 3H).  $^{13}\text{C}$  NMR (126 MHz,  $\text{CDCl}_3$ )  $\delta$  201.4, 160.6, 135.3, 132.2, 126.0, 125.2, 123.6, 123.5, 122.2, 111.5, 62.1, 44.2, 31.7, 29.3, 29.2, 24.7, 22.6, 14.2, 14.1. MS (ESI):  $m/z$  372.2 [M + Na]<sup>+</sup>.

**Ethyl 6-Chloro-3-hexanoyl-1*H*-indole-2-carboxylate (14i, DN441).** The final product was obtained after 3-acylation of indole 1 using synthetic procedure 1. Yellow solid, yield 95%.  $^1\text{H}$  NMR (500 MHz,  $\text{CDCl}_3$ )  $\delta$  9.17 (br s, 1H), 7.85 (d,  $J = 8.7$  Hz, 1H), 7.41 (d,  $J = 1.8$  Hz, 1H), 7.20 (dd,  $J = 8.7, 1.8$  Hz, 1H), 4.45 (q,  $J = 7.1$  Hz, 2H), 3.06 (t,  $J = 7.4$  Hz, 2H), 1.76–1.70 (m, 2H), 1.37 (t,  $J = 7.1$  Hz, 3H), 1.33–1.26 (m, 4H), 0.90–0.88 (m, 3H).  $^{13}\text{C}$  NMR (126 MHz,  $\text{CDCl}_3$ )  $\delta$  201.4, 160.8, 135.4, 132.4, 126.2, 125.5, 123.9, 123.7, 122.4, 111.7, 62.3, 44.4, 31.7, 24.6, 24.6, 22.8, 14.4. MS (ESI):  $m/z$  322.1 [M + H]<sup>+</sup>.

**Ethyl 6-Chloro-3-(2-phenylacetyl)-1*H*-indole-2-carboxylate (14j, DN309).** The final product was obtained after 3-acylation of indole 1 using synthetic procedure 1. Yellow solid, yield 99%.  $^1\text{H}$  NMR (500 MHz,  $\text{CDCl}_3$ )  $\delta$  9.49 (s, 1H), 7.78 (d,  $J = 8.7$  Hz, 1H), 7.36 (s, 1H), 7.28 (d,  $J = 7.2$  Hz, 2H), 7.27–7.20 (m, 3H), 7.15 (d,  $J = 8.7, 1.7$  Hz, 1H), 4.48 (q,  $J = 7.1$  Hz, 2H), 4.45 (s, 2H), 1.43 (t,  $J = 7.1$  Hz, 3H).  $^{13}\text{C}$  NMR (126 MHz,  $\text{CDCl}_3$ )  $\delta$  198.3, 160.5, 135.2, 134.7, 133.2, 129.6, 128.5, 126.8, 126.4, 125.4, (2 $\times$ ) 123.6, 123.5, 121.5, 111.6, 62.2, 50.5, 14.3. MS (ESI):  $m/z$  340.2 [M – H]<sup>+</sup>.

**Ethyl 6-Chloro-3-(2-(*p*-tolyl)acetyl)-1*H*-indole-2-carboxylate (14k, N225).** The final product was obtained after 3-acylation of indole 1 using synthetic procedure 1. White solid, yield 94%.  $^1\text{H}$  NMR (500 MHz,  $\text{CDCl}_3$ )  $\delta$  9.18 (s, 1H), 7.60 (d,  $J = 8.6$  Hz, 1H), 7.42 (s, 1H), 7.21–7.11 (m, 5H), 4.42 (q,  $J = 7.1$  Hz, 2H), 3.62 (s, 2H), 2.33 (s, 3H), 1.42 (t,  $J = 7.1$  Hz, 3H).  $^{13}\text{C}$  NMR (126 MHz,  $\text{CDCl}_3$ )  $\delta$  177.4, 162.2, 137.2, 137.0, 131.3, 130.3, 129.4, 129.2, 128.1, 126.0, 123.5, 121.8, 111.8, 108.7, 61.4, 40.6, 21.1, 14.4. MS (ESI):  $m/z$  378.1 [M + Na]<sup>+</sup>.

**Ethyl 6-Chloro-3-(2-(4-chlorophenyl)acetyl)-1*H*-indole-2-carboxylate (14l, DN522).** The final product was obtained after 3-acylation of indole 1 using synthetic procedure 1. Yellow solid, yield 95%.  $^1\text{H}$  NMR (500 MHz,  $\text{DMSO}-d_6$ )  $\delta$  12.5 (br s, 1H), 7.79 (d,  $J = 8.4$  Hz, 1H), 7.53 (s, 1H), 7.35 (d,  $J = 7.8$  Hz, 2H), 7.25 (d,  $J = 7.8$  Hz, 2H),

7.21 (d,  $J = 8.4$  Hz, 1H), 4.44 (q,  $J = 6.6$  Hz, 2H), 4.37 (s, 2H), 1.36 (t,  $J = 6.6$  Hz, 3H).  $^{13}\text{C}$  NMR (126 MHz,  $\text{DMSO}-d_6$ )  $\delta$  197.1, 161.1, 136.2, 134.8, 132.0, 131.7, 130.4, 128.8, 128.6, 125.1, 123.7, 123.2, 120.1, 112.7, 62.3, 48.9, 14.5. MS (ESI):  $m/z$  374.0 [M – H]<sup>+</sup>.

**Ethyl 6-Chloro-3-(2-(4-fluorophenyl)acetyl)-1*H*-indole-2-carboxylate (14m, DN312).** The final product was obtained after 3-acylation of indole 1 using synthetic procedure 1. Yellow solid, yield 95%.  $^1\text{H}$  NMR (500 MHz,  $\text{CDCl}_3$ )  $\delta$  9.20 (br s, 1H), 7.81 (d,  $J = 8.0$  Hz, 1H), 7.40 (s, 1H), 7.23–7.18 (m, 3H), 6.98–7.01 (m, 2H), 4.50 (q,  $J = 7.2$  Hz, 2H), 4.43 (s, 2H), 1.46 (t,  $J = 7.2$  Hz, 3H).  $^{13}\text{C}$  NMR (126 MHz,  $\text{CDCl}_3$ )  $\delta$  198.3, 160.6, 135.4, 132.7, (2 $\times$ ) 131.4, 126.6, 125.7, 124.0, 123.9, 115.6, 115.5, 111.7, 62.5, 49.6, 40.1, 14.5. MS (ESI):  $m/z$  358.0 [M – H]<sup>+</sup>.

**Ethyl 6-Chloro-3-(3-phenylpropanoyl)-1*H*-indole-2-carboxylate (14n, DN427).** The final product was obtained after 3-acylation of indole 1 using synthetic procedure 1. Red solid, yield 96%.  $^1\text{H}$  NMR (500 MHz,  $\text{CDCl}_3$ )  $\delta$  9.20 (br s, 1H), 7.83 (d,  $J = 8.8$  Hz, 1H), 7.39 (s, 1H), 7.28–7.17 (m, 6H), 4.41 (q,  $J = 7.1$  Hz, 2H), 3.42 (t,  $J = 7.7$  Hz, 2H), 3.09 (t,  $J = 7.7$  Hz, 2H), 1.38 (t,  $J = 7.1$  Hz, 3H).  $^{13}\text{C}$  NMR (126 MHz,  $\text{CDCl}_3$ )  $\delta$  200.1, 160.7, 141.4, 135.4, 134.8, 132.5, (2 $\times$ ) 128.60, 125.5, 124.0, (2 $\times$ ) 123.8, 111.7, 62.4, 45.7, 30.8, 14.4. MS (ESI):  $m/z$  378.1 [M + Na]<sup>+</sup>.

**Ethyl 6-Chloro-1*H*-indole-2-carboxylate (1).**<sup>45,46</sup> White solid, yield 75%.  $^1\text{H}$  NMR (500 MHz,  $\text{CDCl}_3$ )  $\delta$  8.89 (s, 1H), 7.60 (d,  $J = 8.7$  Hz, 1H), 7.42 (s, 1H), 7.20 (d,  $J = 8.7$  Hz, 1H), 7.13 (dd,  $J = 8.7, 0.5$  Hz, 1H), 4.41 (q,  $J = 7.1$  Hz, 2H), 1.43 (t,  $J = 7.1$  Hz, 3H).

**Ethyl 6-Chloro-3-formyl-1*H*-indole-2-carboxylate (2).**<sup>47,48</sup> Yellow solid, yield 85%.  $^1\text{H}$  NMR (500 MHz,  $\text{CDCl}_3$ )  $\delta$  10.7 (s, 1H), 9.34 (br s, 1H), 8.38 (d,  $J = 8.7$  Hz, 1H), 7.45 (s, 1H), 7.30 (d,  $J = 8.7$  Hz, 1H), 4.52 (q,  $J = 7.1$  Hz, 2H), 1.46 (t,  $J = 7.1$  Hz, 3H).

**Ethyl 6-Chloro-3-formyl-1-methyl-1*H*-indole-2-carboxylate (3).**<sup>47</sup> Yellow solid, yield 95%.  $^1\text{H}$  NMR (500 MHz,  $\text{CDCl}_3$ )  $\delta$  10.6 (s, 1H), 8.43 (d,  $J = 8.7$  Hz, 1H), 7.43 (s, 1H), 7.32 (d,  $J = 8.7$  Hz, 1H), 4.53 (q,  $J = 7.1$  Hz, 2H), 1.48 (t,  $J = 7.1$  Hz, 3H).  $^{13}\text{C}$  NMR (126 MHz,  $\text{CDCl}_3$ )  $\delta$  188.4, 161.0, 134.8, 132.6, (2 $\times$ ) 125.1, 123.2, 120.0, (2 $\times$ ) 110.6, 62.5, 32.8, 14.5.

**6-Chloro-3-formyl-1*H*-indole-2-carboxylic Acid (7).**<sup>47</sup> Pink solid, yield 75%.  $^1\text{H}$  NMR (500 MHz,  $\text{CDCl}_3$ )  $\delta$  10.7 (s, 1H), 8.27 (d,  $J = 8.7$  Hz, 1H), 7.57 (d,  $J = 0.5$  Hz, 1H), 7.23 (dd,  $J = 8.7, 0.5$  Hz, 1H).

**tert-Butyl 6-Chloro-1*H*-indole-2-carboxylate (8).**<sup>49</sup> Pink solid, yield 75%.  $^1\text{H}$  NMR (500 MHz,  $\text{CDCl}_3$ )  $\delta$  7.57 (d,  $J = 10$  Hz, 1H), 7.41 (s, 1H), 7.11–7.09 (m, 2H), 1.62 (s, 9H).

**Enzyme Inhibition Studies. Human 15-LOX-1 Screening UV Assay.** The h-15-LOX-1 enzyme was expressed and purified as described before.<sup>32</sup> h-15-LOX-1 activity was determined by the conversion of linoleic acid to 13S-hydroperoxy-9Z,11E-octadecadienoic acid (13(S)-HpODE) ( $\lambda_{\text{max}}$  of 234 nm). The conversion rate was followed by UV absorbance at 234 nm over time. The linear increase in absorbance was used to determine the enzyme's activity. That conversion rate was evaluated at the linear part of the plot before the substrate depletion. The linear part usually covers the first 10–16 min, depending on the enzyme's concentration. The optimum concentration of h-15-LOX-1 was determined by an enzyme activity assay (640-fold dilution). The raw data for the conversion of linoleic acid in the presence (positive control) or absence (blank) of the enzyme using the UV absorbance assay at 234 nm over time are presenting in Figure S1.

The assay buffer consists of 25 mM HEPES titrated to pH 7.5 using a concentrated aqueous solution of NaOH. The substrate, linoleic acid (LA) (Sigma-Aldrich, L1376), was diluted in ethanol to 500  $\mu\text{M}$ . The inhibitor (100 mM in DMSO) was diluted with assay buffer to 125  $\mu\text{M}$ . The inhibitor solution of 80  $\mu\text{L}$  was mixed with 60  $\mu\text{L}$  of assay buffer and 50  $\mu\text{L}$  of 1:160 enzyme solution and incubated for 10 min at rt. After incubation, 10  $\mu\text{L}$  of 500  $\mu\text{M}$  LA was added to the mixture, which resulted in a mixture with a final dilution of the enzyme of 1:640 and 25  $\mu\text{M}$  LA. The linear absorbance increase in the absence of the inhibitor was set to 100%, whereas the absorbance increase in absence of the enzyme was set to 0%. All experiments were performed in triplicate, and the average triplicate values and their standard deviations are plotted. The half-maximal inhibition concentration

(IC<sub>50</sub>) of the inhibitors for h-15-LOX-1 was determined using the same assay. The inhibitor was diluted with assay buffer. Using a serial dilution, the desired concentrations of the inhibitor were obtained, ranging from 0.09 to 50 μM or 0.009 to 20 μM, depending of the inhibitory potency. Data analysis was performed using Microsoft Excel professional plus 2013 and GraphPad Prism 5.01.

**Michaelis–Menten Enzyme Kinetics.** In this kinetics study, 25 mM HEPES buffer, pH 7.5, was used as the assay buffer. The enzyme was diluted 1:160 with assay buffer, and linoleic acid (Sigma-Aldrich, L1376-1G) was diluted with EtOH to 4 mM. LA concentrations ranging from 0.05 to 3 mM were prepared using the 4 mM LA stock solution. Enzyme activity was measured in the absence or presence of fixed concentrations of the inhibitor (0, 1.5, and 3.0 μM). Fifty microliters of the enzyme solution was mixed with 80 μL of inhibitor (25 or 50 μM) and 60 μL of assay buffer and incubated for 10 min at rt. In the absence of the inhibitor, the amount of inhibitor is substituted with assay buffer. Subsequently, 10 μL of LA solution, ranging from 0.05 to 4 mM, was added to the mixture to provide a mixture with a final dilution of the enzyme of 1:640. The mixtures were immediately measured after 5 s of mixing the enzyme with the inhibitor and substrate for 16 min. These experiments were performed in triplicate. The reaction velocities (*v*) were plotted against the substrate concentrations in a Michaelis–Menten plot, and K<sub>m</sub> and V<sub>max</sub> values in the presence of the inhibitor were derived. The reciprocal of the velocities was taken and plotted against the reciprocal of the LA concentration in a Lineweaver–Burk plot. Substrate inhibition was obtained at concentrations above 60 μM. All experiments were performed in triplicate, and the average triplicate values and their standard deviations are plotted. Data analysis was performed using Microsoft Excel professional plus 2013 and GraphPad Prism 5.01.

**Gene Expression Profiling.** Animals. C57BL/6 male mice (weight 20–25 g; age 8–10 weeks) were purchased from Harlan (Zeist, The Netherlands). Animals were maintained on mouse chow and tap water *ad libitum* in a humidity- and temperature-controlled room at 24 °C with a 12 h light/dark cycle. All experiments were performed according to national guidelines and upon approval of the experimental procedures by the local Animal Care and Use Committee of Groningen University, DEC no. 6962A. Mice were randomly assigned to the experimental groups.

**Precision-Cut Lung Slices.** Mouse precision-cut lung slices (PCLS) were prepared as previously described for guinea pig with the following modifications.<sup>50</sup> Male mice were anesthetized by a subcutaneous injection of ketamin (75 mg/kg, Alfasan, Woerden, The Netherlands) and dexdomitor (0.5 mg/kg, Orion Pharma, Mechelen, Belgium). Subsequently, the trachea was cannulated, and the animal was exsanguinated by cutting the jugular vein, after which the lungs were filled trough the cannula with 1.5 mL of a low melting-point agarose solution (1.5% final concentration (Gerbu Biotechnik GmbH, Wieblingen, Germany) in CaCl<sub>2</sub> (0.9 mM), MgSO<sub>4</sub> (0.4 mM), KCl (2.7 mM), NaCl (58.2 mM), NaH<sub>2</sub>PO<sub>4</sub> (0.6 mM), glucose (8.4 mM), NaHCO<sub>3</sub> (13 mM), HEPES (12.6 mM, Gibco by Life Technologies, Bleiswijk, The Netherlands), sodium pyruvate (0.5 mM, GE Healthcare Life Sciences, Eindhoven, The Netherlands), glutamine (1 mM, Gibco by Life Technologies), MEM–amino acid mixture (1:50, Gibco by Life Technologies), and MEM–vitamins mixture (1:100, Gibco by Life Technologies), pH 7.2). The lungs were placed on ice for 15 min to solidify the agarose for slicing. The lobes were separated, and tissue cores were prepared of the individual lobes, after which the lobes were sliced at a thickness of 250 μm in medium composed of CaCl<sub>2</sub> (1.8 mM), MgSO<sub>4</sub> (0.8 mM), KCl (5.4 mM), NaCl (116.4 mM), NaH<sub>2</sub>PO<sub>4</sub> (1.2 mM), glucose (16.7 mM), NaHCO<sub>3</sub> (26.1 mM), and HEPES (25.2 mM), pH 7.2, using a tissue slicer (Compresstome VF-300 microtome, Precisionary Instruments, San Jose, CA, USA). Tissue slices were incubated at 37 °C in a humid atmosphere under 5% CO<sub>2</sub>/95% air. In order to remove the agarose and cell debris from the tissue, slices were washed every 30 min (four times in total) in medium composed of CaCl<sub>2</sub> (1.8 mM), MgSO<sub>4</sub> (0.8 mM), KCl (5.4 mM), NaCl (116.4 mM), NaH<sub>2</sub>PO<sub>4</sub> (1.2 mM), glucose (16.7 mM), NaHCO<sub>3</sub> (26.1 mM), HEPES (25.2 mM), sodium pyruvate (1 mM), glutamine (2 mM), MEM–amino acid

mixture (1:50), MEM–vitamins mixture (1:100), penicillin (100 U/mL, Gibco by Life Technologies), and streptomycin (100 μg/mL, Gibco by Life Technologies), pH 7.2. Chemicals to prepare the media described above were obtained from Sigma-Aldrich (Zwijndrecht, The Netherlands) unless stated otherwise and were of analytical grade.

**Treatment of Lung Slices.** PCLS were incubated in Dulbecco's modified Eagle's medium (DMEM, Gibco by Life Technologies) supplemented with sodium pyruvate (1 mM), MEM–nonessential amino acid mixture (1:100, Gibco by Life Technologies), gentamycin (45 μg/mL, Gibco by Life Technologies), penicillin (100 U/mL), streptomycin (100 μg/mL), and amphotericin B (1.5 μg/mL, Gibco by Life Technologies). Slices were cultured at 37 °C in a humidified atmosphere under 5% CO<sub>2</sub>/95% air in 12-well tissue culture plates (Costar Europe, Badhoevedorp, The Netherlands), using 3 slices per well. Slices were treated with LOX inhibitor (LOXi) 14d at a final concentration of 1–500 nM for 20 h and were coincubated with 10 μM Linoleic acid (L1376; Sigma-Aldrich). During the last 4 h of the experiments, tissue slices were stimulated with 10 ng/mL lipopolysaccharide (LPS, *Escherichia coli*, serotype 0111:B4; Sigma-Aldrich) and 10 ng/mL interferon gamma (IFN $\gamma$ , cat. no. 315-05; PeproTech, Hamburg, Germany).

**Assessment of Tissue Viability Using Lactate Dehydrogenase.** To assess the viability of the PCLS subjected to increasing concentrations 14d, the amount of lactate dehydrogenase (LDH) released from the tissue slices into the incubation medium was analyzed. Maximal LDH release was determined by lysing 3 slices with 1% Triton X-100 for 30 min at 37 °C at the start of the experiments. Supernatants were stored at –80 °C. LDH release was determined using an assay form Roche Diagnostics (Mannheim, Germany) and was measured using a Hitachi automatic analyzer (Modular Analytics, Roche Diagnostics). LDH release from the PCLS into the incubation medium was plotted relative to maximal LDH release.

**Cell Culture and LOXi Treatment.** RAW 264.7 murine macrophage cells were obtained from ATCC (Wesel, Germany) and cultured in plastic tissue culture plates or flasks at 37 °C under 5% CO<sub>2</sub>/95% air in DMEM + GlutaMAX (Gibco by Life Technologies) supplemented with 10% (v/v) heat inactivated fetal bovine serum (FBS; Invitrogen, Breda, The Netherlands), 2 mM additional GlutaMAX (Gibco by Life Technologies), 100 U/mL penicillin, and 100 μg/mL streptomycin. RAW 264.7 cells were used between passages 7 and 16.

To obtain identical cell densities at the start of the experiment, RAW 264.7 cells were seeded at 20 000 cells/cm<sup>2</sup> in 12-well tissue culture plates 1 day prior to the experiment. Cells were treated with the LOXi 14d (final concentration, 1–500 nM) for 20 h and were coincubated with 10 μM linoleic acid. Cells were stimulated with 10 ng/mL LPS and IFN $\gamma$  for the last 4 h of the experiment.

**Gene Expression Analysis by RT-qPCR.** RAW 264.7 cells and PCLS were washed twice with ice-cold DPBS (Gibco by Life Technologies), and total RNA was isolated from RAW 264.7 cells using the SV total RNA isolation system (Promega, Leiden, The Netherlands) and from PCLS using the Maxwell 16 LEV simplyRNA tissue kit (Promega), both of which were performed according to the protocol of the manufacturer. RNA integrity was determined by 28S/18S ratio detection on an agarose gel, which was consistently found to be intact. For gene expression analysis, RNA was reverse-transcribed using a reverse-transcription kit (Promega). Subsequently, 10 ng of cDNA was applied for each real-time PCR, which was performed on an ABI Prism 7900HT sequence detection system (Applied Biosystems, Nieuwerkerk a/d IJssel, The Netherlands). The primers for IL-1 $\beta$  (Mm00434228\_m1), IL-6 (Mm00446190\_m1), IL-10 (Mm00439614\_m1), IL-12 (Mm00434174\_m1), and GAPDH (Mm99999915\_g1) were purchased as Assay-on-Demand (Applied Biosystems). For each sample, the real-time PCR reactions were performed in duplicate or triplicate, and the averages of the obtained C<sub>t</sub> values were used for further calculations. Gene expression levels were normalized to the expression of the reference gene glyceraldehyde-3-phosphate dehydrogenase (GAPDH), which was not influenced by the experimental conditions, resulting in the ΔC<sub>t</sub> value. Gene expression levels were calculated by the comparative C<sub>t</sub> method (2<sup>−ΔΔC\_t</sup>).<sup>51</sup>

**Statistical Analysis.** Statistical analysis of the results was performed by a two-tailed unpaired Student's *t*-test, assuming equal variances to compare two replicate groups. Analysis of differences between multiple replicate groups was analyzed with one-way ANOVA followed by Tukey's *posthoc* analysis. *p* values < 0.05 were considered to be significant. Data were analyzed with GraphPad Prism (GraphPad software 5.00, San Diego, CA, USA).

## ■ ASSOCIATED CONTENT

### Supporting Information

The Supporting Information is available free of charge on the ACS Publications website at DOI: [10.1021/acs.jmedchem.Sb01121](https://doi.org/10.1021/acs.jmedchem.Sb01121).

<sup>1</sup>H and <sup>13</sup>C NMR spectra data, data set of focused library (Table S1), screening results (Table S2), enzyme kinetic parameters (Table S3), positive and negative control of enzymatic conversion (Figure S1), IC<sub>50</sub> graphs (Figure S2), steady-state kinetic characterization of 15-LOX-1 (Figure S3), and molecular modeling docking poses (Figures S4 and S5) ([PDF](#)).

## ■ AUTHOR INFORMATION

### Corresponding Author

\*Phone: +31-5-3638030. Fax: +31-5-3637953. E-mail: [f.j.dekker@rug.nl](mailto:f.j.dekker@rug.nl).

### Notes

The authors declare no competing financial interest.

## ■ ACKNOWLEDGMENTS

We acknowledge the European Research Counsel for providing an ERC starting grant (309782) and The Netherlands Organisation for Scientific Research (NWO) for providing a VIDI grant (016.122.302) to F.J.D. We acknowledge the COST action "biomimetic radical chemistry" CM1201. The work (C.G.N. and A.D.) was financially supported from the NIH (1R01GM097082-01) and by Innovative Medicines Initiative (grant agreement no. 115489). We acknowledge Prof. Dr. Reinoud Gosens (Department of Molecular Pharmacology, University of Groningen) for his support with *ex vivo* experiments. We also acknowledge T. Holman (University of California, Santa Cruz) for providing the h-15-LOX-1 plasmid.

## ■ ABBREVIATIONS USED

BOC, *tert*-butyl carbonate; DCM, dichloromethane; DMF, dimethylformamide; EtOAc, ethyl acetate; EtOH, ethanol; Et<sub>2</sub>O, diethyl ether; rt, room temperature

## ■ REFERENCES

- Barnes, P. J. Immunology of Asthma and Chronic Obstructive Pulmonary Disease. *Nat. Rev. Immunol.* **2008**, *8* (3), 183–192.
- Corey, E. J.; Czakó, B.; Kürti, L. *Molecules and Medicine*; WILEY-VCH Verlag: Hoboken, NJ, 2007.
- Boorsma, C. E.; Draijer, C.; Melgert, B. N. Macrophage Heterogeneity in Respiratory Diseases. *Mediators Inflammation* **2013**, 769214.
- Gordon, S.; Taylor, P. R. Monocyte and Macrophage Heterogeneity. *Nat. Rev. Immunol.* **2005**, *5* (12), 953–964.
- Gordon, S.; Plüddemann, A.; Martinez Estrada, F. Macrophage Heterogeneity in Tissues: Phenotypic Diversity and Functions. *Immunol. Rev.* **2014**, *262* (1), 36–55.
- Schneberger, D.; Aharonson-Raz, K.; Singh, B. Monocyte and Macrophage Heterogeneity and Toll-like Receptors in the Lung. *Cell Tissue Res.* **2011**, *343*, 97–106.

(7) Brash, A. R. Lipoxygenases: Occurrence, Functions, Catalysis, and Acquisition of Substrate. *J. Biol. Chem.* **1999**, *274* (34), 23679–23682.

(8) Kulkarni, A. Lipoxygenase-a Versatile Biocatalyst for Biotransformation of Endobiotics and Xenobiotics. *Cell. Mol. Life Sci.* **2001**, *58* (12–13), 1805–1825.

(9) Haeggström, J. Z.; Funk, C. D. Lipoxygenase and Leukotriene Pathways: Biochemistry, Biology, and Roles in Disease. *Chem. Rev.* **2011**, *111* (10), 5866–5898.

(10) Joo, Y.-C.; Oh, D.-K. Lipoxygenases: Potential Starting Biocatalysts for the Synthesis of Signaling Compounds. *Biotechnol. Adv.* **2012**, *30* (6), 1524–1532.

(11) Samuelsson, B.; Dahlen, S.; Lindgren, J.; Rouzer, C.; Serhan, C. Leukotrienes and Lipoxins: Structures, Biosynthesis, and Biological Effects. *Science* **1987**, *237* (4819), 1171–1176.

(12) Sigal, E.; Dicharry, S.; Highland, E.; Finkbeiner, W. E. Cloning of Human Airway 15-Lipoxygenase: Identity to the Reticulocyte Enzyme and Expression in Epithelium. *Am. J. Physiol.* **1992**, *262*, L392–L398.

(13) Conrad, D. J.; Kuhn, H.; Mulkins, M.; Highland, E.; Sigal, E. Specific Inflammatory Cytokines Regulate the Expression of Human Monocyte 15-Lipoxygenase. *Proc. Natl. Acad. Sci. U. S. A.* **1992**, *89* (1), 217–221.

(14) Mabalirajan, U.; Rehman, R.; Ahmad, T.; Kumar, S.; Leishangthem, G. D.; Singh, S.; Dinda, A. K.; Biswal, S.; Agrawal, A.; Ghosh, B. 12/15-Lipoxygenase Expressed in Non-Epithelial Cells Causes Airway Epithelial Injury in Asthma. *Sci. Rep.* **2013**, *3*, 1540.

(15) Middleton, M. K.; Rubinstein, T.; Pure, E. Cellular and Molecular Mechanisms of the Selective Regulation of IL-12 Production by 12/15-Lipoxygenase. *J. Immunol.* **2006**, *176* (1), 265–274.

(16) Levy, B. D.; Serhan, C. N. Resolution of Acute Inflammation in the Lung. *Annu. Rev. Physiol.* **2014**, *76*, 467–492.

(17) Okunishi, K.; Peters-Golden, M. Leukotrienes and Airway Inflammation. *Biochim. Biophys. Acta, Gen. Subj.* **2011**, *1810* (11), 1096–1102.

(18) Zhao, J.; O'Donnell, V. B.; Balzar, S.; St. Croix, C. M.; Trudeau, J. B.; Wenzel, S. E. 15-Lipoxygenase 1 Interacts with Phosphatidylethanolamine-Binding Protein to Regulate MAPK Signaling in Human Airway Epithelial Cells. *Proc. Natl. Acad. Sci. U. S. A.* **2011**, *108* (34), 14246–14251.

(19) Mabalirajan, U.; Rehman, R.; Ahmad, T.; Kumar, S.; Singh, S.; Leishangthem, G. D.; Aich, J.; Kumar, M.; Khanna, K.; Singh, V. P.; Dinda, A. K.; Biswal, S.; Agrawal, A.; Ghosh, B. Linoleic Acid Metabolite Drives Severe Asthma by Causing Airway Epithelial Injury. *Sci. Rep.* **2013**, *3*, 1349.

(20) Lindley, A. R.; Crapster-Pregont, M.; Liu, Y.; Kuperman, D. A. 12/15-Lipoxygenase Is an Interleukin-13 and Interferon- $\Gamma$  Counter-regulated-Mediator of Allergic Airway Inflammation. *Mediators Inflammation* **2010**, 727305.

(21) Sendobry, S. M.; Cornicelli, J. A.; Welch, K.; Bocan, T.; Tait, B.; Trivedi, B. K.; Colbry, N.; Dyer, R. D.; Feinmark, S. J.; Daugherty, A. Attenuation of Diet-Induced Atherosclerosis in Rabbits with a Highly Selective 15-Lipoxygenase Inhibitor Lacking Significant Antioxidant Properties. *Br. J. Pharmacol.* **1997**, *120* (7), 1199–1206.

(22) Weinstein, D. S.; Liu, W.; Gu, Z.; Langevine, C.; Ngu, K.; Fadnis, L.; Combs, D. W.; Sitkoff, D.; Ahmad, S.; Zhuang, S.; Chen, X.; Wang, F.-L.; Loughney, D. A.; Atwal, K. S.; Zahler, R.; Macor, J. E.; Madsen, C. S.; Murugesan, N. Tryptamine and Homotryptamine-Based Sulfonamides as Potent and Selective Inhibitors of 15-Lipoxygenase. *Bioorg. Med. Chem. Lett.* **2005**, *15* (5), 1435–1440.

(23) Ngu, K.; Weinstein, D. S.; Liu, W.; Langevine, C.; Combs, D. W.; Zhuang, S.; Chen, X.; Madsen, C. S.; Harper, T. W.; Ahmad, S.; Robl, J. a Pyrazole-Based Sulfonamide and Sulfamides as Potent Inhibitors of Mammalian 15-Lipoxygenase. *Bioorg. Med. Chem. Lett.* **2011**, *21* (14), 4141–4145.

(24) Rai, G.; Kenyon, V.; Jadhav, A.; Schultz, L.; Armstrong, M.; Jameson, J. B.; Hoobler, E.; Leister, W.; Simeonov, A.; Holman, T. R.; Maloney, D. J. Discovery of Potent and Selective Inhibitors of Human

- Reticulocyte 15-Lipoxygenase-1. *J. Med. Chem.* **2010**, *53* (20), 7392–7404.
- (25) Rai, G.; Joshi, N.; Jung, J. E.; Liu, Y.; Schultz, L.; Yasgar, A.; Perry, S.; Diaz, G.; Zhang, Q.; Kenyon, V.; Jadhav, A.; Simeonov, A.; Lo, E. H.; van Leyen, K.; Maloney, D. J.; Holman, T. R. Potent and Selective Inhibitors of Human Reticulocyte 12/15-Lipoxygenase as Anti-Stroke Therapies. *J. Med. Chem.* **2014**, *57* (10), 4035–4048.
- (26) Weinstein, D. S.; Liu, W.; Ngu, K.; Langervine, C.; Combs, D. W.; Zhuang, S.; Chen, C.; Madsen, C. S.; Harper, T. W.; Robl, J. A. Discovery of Selective Imidazole-Based Inhibitors of Mammalian 15-Lipoxygenase: Highly Potent against Human Enzyme within a Cellular Environment. *Bioorg. Med. Chem. Lett.* **2007**, *17* (18), 5115–5120.
- (27) Gundersen, L.-L.; Malterud, K. E.; Negussie, A. H.; Rise, F.; Teklu, S.; Østby, O. B. Indolizines as Novel Potent Inhibitors of 15-Lipoxygenase. *Bioorg. Med. Chem.* **2003**, *11* (24), 5409–5415.
- (28) Mahdavi, M.; Shirazi, M. S.; Taherkhani, R.; Saeedi, M.; Alipour, E.; Moghadam, F. H.; Moradi, A.; Nadri, H.; Emami, S.; Firoozpour, L.; Shafee, A.; Foroumadi, A. Synthesis, Biological Evaluation and Docking Study of 3-Aroyl-1-(4-Sulfamoylphenyl)thiourea Derivatives as 15-Lipoxygenase Inhibitors. *Eur. J. Med. Chem.* **2014**, *82*, 308–313.
- (29) Asghari, T.; Bakavoli, M.; Rahimizadeh, M.; Eshghi, H.; Saberi, S.; Karimian, A.; Hadizadeh, F.; Ghandadi, M. Synthesis and Evaluation of a New Series of 3,5-bis((5-Bromo-6-Methyl-2-T-Aminopyrimidin-4-Yl)thio)-4H-1,2,4-Triazol-4-Amines and Their Cyclized Products “Pyrimidinylthio Pyrimidotriazolothiadiazines” as 15-Lipo-Oxygenase Inhibitors. *Chem. Biol. Drug Des.* **2015**, *85* (2), 216–224.
- (30) Wisastr, R.; Ghizzoni, M.; Boltjes, A.; Haisma, H. J.; Dekker, F. J. Anacardic Acid Derived Salicylates Are Inhibitors or Activators of Lipoxygenases. *Bioorg. Med. Chem.* **2012**, *20* (16), 5027–5032.
- (31) Wisastr, R.; Kok, P. A. M.; Eleftheriadis, N.; Baumgartner, M. P.; Camacho, C. J.; Haisma, H. J.; Dekker, F. J. Discovery of a Novel Activator of 5-Lipoxygenase from an Anacardic Acid Derived Compound Collection. *Bioorg. Med. Chem.* **2013**, *21* (24), 7763–7778.
- (32) Eleftheriadis, N.; Thee, S.; Te Biesebeek, J.; van der Wouden, P.; Baas, B.-J.; Dekker, F. J. Identification of 6-Benzoylsalicylates as a Novel Class of Inhibitors of 15-Lipoxygenase-1. *Eur. J. Med. Chem.* **2015**, *94*, 265–275.
- (33) Rai, G.; Joshi, N.; Jung, J. E.; Liu, Y.; Schultz, L.; Yasgar, A.; Perry, S.; Diaz, G.; Zhang, Q.; Kenyon, V.; Jadhav, A.; Simeonov, A.; Lo, E. H.; van Leyen, K.; Maloney, D. J.; Holman, T. R. Potent and Selective Inhibitors of Human Reticulocyte 12/15-Lipoxygenase as Anti-Stroke Therapies. *J. Med. Chem.* **2014**, *57* (10), 4035–4048.
- (34) Whittle, A.; Young, E. H. P. The Synthesis and Pharmacological Activity of Some Chloro- $\alpha$ -Alkyltryptamines. *J. Med. Chem.* **1963**, *6*, 378–380.
- (35) JOSHI, K. C.; PATHAK, V. N.; CHAND, P. Synthesis and CNS Activity of Some Fluorine Containing 3-Indolylglyoxamides and Tryptamines. *Agric. Biol. Chem.* **1978**, *42*, 1723–1726.
- (36) Ottoni, O.; Neder, a V; Dias, a K.; Cruz, R. P.; Aquino, L. B. Acylation of Indole under Friedel-Crafts Conditions—an Improved Method to Obtain 3-Acylindoles Regioselectively. *Org. Lett.* **2001**, *3* (7), 1005–1007.
- (37) Gillmor, S. A.; Villaseñor, A.; Fletterick, R.; Sigal, E.; Browner, M. F. The Structure of Mammalian 15-Lipoxygenase Reveals Similarity to the Lipases and the Determinants of Substrate Specificity. *Nat. Struct. Biol.* **1997**, *4* (12), 1003–1009.
- (38) Abad-Zapatero, C.; Metz, J. Ligand Efficiency Indices as Guideposts for Drug Discovery. *Drug Discovery Today* **2005**, *10* (7), 464–469.
- (39) Kuntz, I. D.; Chen, K.; Sharp, K. A.; Kollman, P. A. The Maximal Affinity of Ligands. *Proc. Natl. Acad. Sci. U. S. A.* **1999**, *96*, 9997–10002.
- (40) Hopkins, A. L.; Keserü, G. M.; Leeson, P. D.; Rees, D. C.; Reynolds, C. H. The Role of Ligand Efficiency Metrics in Drug Discovery. *Nat. Rev. Drug Discovery* **2014**, *13* (2), 105–121.
- (41) Abad-Zapatero, C. Ligand Efficiency Indices for Effective Drug Discovery. *Expert Opin. Drug Discovery* **2007**, *2* (4), 469–488.
- (42) Hackett, T. L.; Holloway, R.; Holgate, S. T.; Warner, J. A. Dynamics of pro-Inflammatory and Anti-Inflammatory Cytokine Release during Acute Inflammation in Chronic Obstructive Pulmonary Disease: An Ex Vivo Study. *Respir. Res.* **2008**, *9*, 47.
- (43) Takanashi, S.; Hasegawa, Y.; Kanehira, Y.; Yamamoto, K.; Fujimoto, K.; Satoh, K.; Okamura, K. Interleukin-10 Level in Sputum Is Reduced in Bronchial Asthma, COPD and in Smokers. *Eur. Respir. J.* **1999**, *14* (2), 302–308.
- (44) Bijiiga, E.; Martino, A. T. Interleukin-10 (IL-10) regulatory cytokine and its clinical consequences. *J. Clin. Cell. Immunol.* **2013**, *S1*, 007.
- (45) Wang, R.; Shi, H.-F.; Zhao, J.-F.; He, Y.-P.; Zhang, H.-B.; Liu, J.-P. Design, Synthesis and Aromatase Inhibitory Activities of Novel Indole-Imidazole Derivatives. *Bioorg. Med. Chem. Lett.* **2013**, *23* (6), 1760–1762.
- (46) Louvet, P.; Lallement, G.; Pernot-Marino, I.; Luu-Duc, C.; Blanchet, G. Novel Benzimidazoles as Ligands for the Strychnine-Insensitive N-Methyl-D-Aspartate-Linked Glycine Receptor. *Eur. J. Med. Chem.* **1993**, *28* (1), 71–75.
- (47) Doemling, A.; Holak, T. Novel p53-mdm2/p53-mdm4 Antagonists to Treat Proliferative Disease. Patent WO 201106650 A2, September 1, 2011.
- (48) Boettcher, A.; Buschmann, N.; Furet, P.; Groell, J. M.; Kallen, J.; Hergovich, L. J.; Masuya, K.; Mayr, L.; Vaupel, A. 3-Imidazolyl-Indoles for the Treatment of Proliferative Diseases. Patent WO 2008119741 A2, October 9, 2008.
- (49) Wright, S. W.; Hageman, D. L.; Wright, A. S.; McClure, L. D. Convenient Preparations of T-Butyl Esters and Ethers from T-Butanol. *Tetrahedron Lett.* **1997**, *38* (42), 7345–7348.
- (50) Oenema, T. A.; Maarsingh, H.; Smit, M.; Groothuis, G. M. M.; Meurs, H.; Gosens, R. Bronchoconstriction Induces TGF-B Release and Airway Remodelling in Guinea Pig Lung Slices. *PLoS One* **2013**, *8* (6), e65580.
- (51) Livak, K. J.; Schmittgen, T. D. Analysis of Relative Gene Expression Data Using Real-Time Quantitative PCR and the 2(-Delta Delta C(T)) Method. *Methods* **2001**, *25*, 402–408.